

1 **Estimates of ikaite export from sea ice to the underlying seawater in a sea**
2 **ice-seawater mesocosm**

3 Geilfus N.-X.^{1,2}, Galley R. J.¹, Else B. G. T.³, Campbell K.¹, Papakyriakou T.¹, Crabeck O.¹, Lemes M.¹, Delille
4 B.⁴, Rysgaard S.^{1,2,5}

5 ¹ Centre for Earth Observation Science, Department of Environment and Geography, University of Manitoba,
6 Winnipeg, Canada

7 ² Arctic Research Centre, Aarhus University, Aarhus, Denmark

8 ³ Department of Geography, University of Calgary, Calgary, Canada

9 ⁴ Unité d’Océanographie Chimique, Université de Liège, Liège, Belgium

10 ⁵ Greenland Climate Research Centre, Greenland Institute of Natural Resources, Nuuk, Greenland

11 **1. Abstract**

12 The precipitation of ikaite and its fate within sea ice is still poorly understood. We quantify temporal
13 inorganic carbon dynamics in sea ice from initial formation to its melt in a sea ice-seawater mesocosm
14 pool from 11 to 29 January 2013. Based on measurements of total alkalinity (TA) and total dissolved
15 inorganic carbon (TCO_2), the main processes affecting inorganic carbon dynamics within sea ice were
16 ikaite precipitation and CO_2 exchange with the atmosphere. In the underlying seawater, the dissolution of
17 ikaite was the main process affecting inorganic carbon dynamics. Sea ice acted as an active layer,
18 releasing CO_2 to the atmosphere during the growth phase, taking up CO_2 as it melted and exporting both
19 ikaite and TCO_2 into the underlying seawater during the whole experiment. Ikaite precipitation of up to
20 $167 \mu\text{mol kg}^{-1}$ within sea ice was estimated while its export and dissolution into the underlying seawater
21 was responsible for a TA increase of 64 to $66 \mu\text{mol kg}^{-1}$ in the water column. The export of TCO_2 from
22 sea ice to the water column increased the underlying seawater TCO_2 by $43.5 \mu\text{mol kg}^{-1}$, suggesting that
23 almost all of the TCO_2 that left the sea ice was exported to the underlying seawater. The export of ikaite
24 from the ice to the underlying seawater was associated with brine rejection during sea ice growth,
25 increased vertical connectivity in sea ice due to the upward percolation of seawater, and meltwater
26 flushing during sea ice melt. Based on the change in TA in the water column around the onset of sea ice
27 melt, more than half of the total ikaite precipitated in the ice during sea ice growth was still contained in
28 the ice when the sea ice began to melt. Ikaite crystal dissolution in the water column kept the seawater
29 pCO_2 undersaturated with respect to the atmosphere in spite of increased salinity, TA, and TCO_2
30 associated with sea ice growth. Results indicate that ikaite export from sea ice and its dissolution in the

31 underlying seawater can potentially hamper the effect of oceanic acidification on the aragonite saturation
32 state ($\Omega_{\text{aragonite}}$) in fall and winter in ice-covered areas, at the time when $\Omega_{\text{aragonite}}$ is smallest.

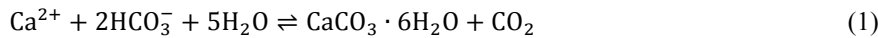
33 **2. Introduction**

34 Currently, each year, 7 Pg of anthropogenic carbon are released to the atmosphere, 29% of which is
35 estimated to be taken up by the Oceans through physical, chemical and biological processes (Sabine et al.,
36 2004). The Arctic Ocean are taking up -66 to -199 Tg C year⁻¹, contributing 5-14% to the global ocean
37 CO₂ uptake (Bates and Mathis, 2009), primarily through primary production and surface cooling
38 (MacGilchrist et al., 2014). However, polar ocean CO₂ uptake estimates consider sea ice as an
39 impermeable barrier, ignoring the potential role of ice-covered areas on gas exchange between the ocean
40 and atmosphere. Recent studies have shown that sea ice covered areas participate in the variable
41 sequestration of atmospheric CO₂ into the mixed layer below the ice (e.g. Papakyriakou and Miller 2011;
42 Geilfus et al., 2012; Nomura et al., 2013; Delille et al., 2014; Geilfus et al., 2014; 2015). Studies are
43 required to elucidate the processes responsible as well as their magnitudes both temporally and spatially.

44 The carbonate chemistry in sea ice and brine is spatially and temporally variable, which leads to
45 complex CO₂ dynamics with the potential to affect the air-sea CO₂ flux (Parmentier et al., 2013). Release
46 of CO₂ from sea ice to the atmosphere has been reported during sea ice formation from open water
47 (Geilfus et al., 2013a) and in winter (Miller et al., 2011; Fransson et al., 2013) while uptake of CO₂ by sea
48 ice from the atmosphere has been reported after sea ice melt onset (e.g. Semiletov et al., 2004; Nomura et
49 al., 2010; Geilfus et al., 2012; Nomura et al., 2013; Fransson et al., 2013; Geilfus et al., 2014; 2015). In
50 combination, these works suggest that the temporal cycle of sea ice formation and melt affects
51 atmospheric CO₂ uptake by the ocean in variable ways. Sea ice may also act as an important control on
52 the partial pressure of CO₂ ($p\text{CO}_2$) in the sea surface through a sea ice pump (Rysgaard et al., 2007).
53 During the earliest stages of sea ice formation, a small fraction of CO₂-supersaturated brine is expelled
54 upward onto the ice surface promoting a release of CO₂ to the atmosphere (Geilfus et al., 2013a). As sea
55 ice forms and grows thicker, salts are partly rejected from the sea ice to the underlying seawater and
56 partly trapped within the sea ice structure, concentrated in brine pockets, tubes and channels. As a result,
57 the concentration of dissolved salts, including inorganic carbon, increase within the brine and promote the
58 precipitation of calcium carbonate crystals such as ikaite ($\text{CaCO}_3 \cdot 6\text{H}_2\text{O}$) (Marion 2001). These crystals
59 have been reported in both natural (Dieckmann et al., 2008; Nomura et al., 2013, Søgaard et al., 2013)

60 and experimental sea ice (Geilfus et al., 2013b; Rysgaard et al., 2014) and have been suggested to be a
61 key component of the carbonate system (Rysgaard et al., 2007; Fransson et al., 2013; Delille et al., 2014).

62 During ikaite precipitation within sea ice, TA in brine is reduced by 2 moles due to the reduction of
63 bicarbonate (HCO_3^-) while TCO_2 in brine is only reduced by 1 mole (equation 1 to 3).



$$65 \quad \text{TCO}_2 = [\text{HCO}_3^-] + [\text{CO}_3^{2-}] + [\text{CO}_2] \quad (2)$$

$$66 \quad \text{TA} = [\text{HCO}_3^-] + 2[\text{CO}_3^{2-}] + [\text{B(OH)}_4^-] + [\text{OH}^-] - [\text{H}^+] \quad (3)$$

67 The specific conditions leading to ikaite precipitation as well as the fate of these precipitates in sea ice are
68 still not fully understood. Ikaite crystals may remain within the ice structure while the CO_2 formed during
69 their precipitation is likely rejected with dense brine to the underlying seawater and sequestered below the
70 mixed layer. During sea ice melt, the dissolution of these crystals triggered by increased ice temperatures
71 and decreased bulk ice salinity will consume CO_2 and drive a CO_2 uptake from the atmosphere to the ice.
72 Such mechanism could be an effective sea ice pump of atmospheric CO_2 (Delille et al., 2014). In
73 addition, ikaite stored in the ice matrix could become a source of TA to the near-surface ocean upon its
74 subsequent dissolution during sea ice melt (Rysgaard et al., 2007; 2009).

75 The main air-sea fluxes of CO_2 and TCO_2 are driven by brine rejection to the underlying seawater and
76 its contribution to intermediate and deep-water formation (Semiletov et al., 2004; Rysgaard et al., 2007,
77 2009; Fransson et al., 2013) or below sea ice in ice tank studies (e.g. Killawee et al., 1998 and
78 Papadimitriou et al., 2004). As sea ice thickens, reduced near-surface ice temperatures result in reduced
79 brine volume content, increased brine salinity and increased solute concentration in the brine. In the
80 spring-summer, as the ice temperature increases, sea ice brine volume increases and sea ice becomes
81 vertically permeable to liquid (Golden et al., 2007), enhancing the potential CO_2 exchange between the
82 atmosphere, sea ice and ocean. Eventually internal ice melt promotes brine dilution, which decreases
83 brine salinity, TA, TCO_2 , and leads to lower $p\text{CO}_2$ in the brine. In addition, the dissolution of ikaite
84 decreases brine $p\text{CO}_2$ (Eq. 1) (Geilfus et al., 2012; 2015). These conditions all favour sea ice as a sink for
85 atmospheric CO_2 (Nomura et al., 2010; Geilfus et al., 2012; Nomura et al., 2013; Geilfus et al., 2015).
86 Melting sea ice stratifies surface seawater leading to decreased TA, TCO_2 and $p\text{CO}_2$, in the sea surface,
87 enhancing air-sea CO_2 fluxes (Rysgaard et al., 2007; 2009).

88 Although we now have a basic understanding of the key mechanisms of carbon cycling in sea ice,
89 significant unknowns remain. One of the major unknowns is the fate of ikaite, $T\text{CO}_2$ and CO_2 released
90 from sea ice during winter. It is unclear what proportion of precipitated ikaite crystals in sea ice remain in
91 the matrix to be released upon melt or what proportion are expelled with brine drainage during ice
92 formation and growth. Examining the chemical signatures of the water column beneath sea ice may
93 provide an indication of the importance of the different processes. However, the signal of carbon
94 components released from 1-2 meters of sea ice growth is difficult to detect in a water column several
95 hundred meters deep.

96 In this study, we followed the evolution of the inorganic carbon dynamics within experimental sea ice
97 from sea ice formation to melt in a sea ice-seawater mesocosm pool ($\sim 435 \text{ m}^3$). The benefits of this type
98 of environment are multiple. An artificial pool equipped with a movable bridge makes it possible to
99 collect undisturbed samples from thin growing sea ice. We gain the ability to carefully track carbonate
100 parameters in the ice, in the atmosphere, and in the underlying seawater, while growing sea ice in a large
101 volume of seawater, so that conditions closely mimic the natural system. During this experiment, we
102 examined physical and chemical processes, in the absence of biology, responsible for changes in the
103 inorganic carbon system of sea ice and the underlying seawater and quantify fluxes of inorganic carbon
104 between the atmosphere, sea ice and the water column. We also discuss that dissolution of ikaite crystals
105 exported from sea ice in the underlying seawater can potentially hamper the effect of oceanic
106 acidification on $\Omega_{\text{aragonite}}$.

107 3. Site description, sampling and analysis

108 The Sea-ice Environmental Research Facility (SERF) is an in-ground outdoor concrete pool of 18.3 m
109 by 9.1 m in surface area and 2.6 m deep exposed to ambient temperatures, winds and solar radiation (by
110 retracting its roof, Fig. 1). The weather conditions in the region are conducive to sea ice growth for
111 several months every winter. Prior to the experiment, the pool is filled with artificial seawater (ASW)
112 made by dissolving large quantities of various rock salts into local groundwater to mimic the major
113 composition of natural seawater (see Rysgaard et al., (2014) for exact composition of the ASW). Sea ice
114 is melted in the pool by circulating heated ethylene glycol through a closed-loop hose located at the
115 bottom of the pool, allowing successive ice growth/melt experiments to be carried out during one winter.
116 The experimental sea ice and brine exhibit similar physical and chemical properties to those observed in
117 natural Arctic sea ice (Geilfus et al., 2013; Hare et al., 2013). The experiment described herein was

118 initiated from open water conditions on 11 January 2013 when the heater was turned off. Sea ice grew
119 until 26 January when the heat was turned back on. The experiment ended on 30 January when the pool
120 was 20% ice-free.

121 Four 375 W pumps were installed on the bottom of the pool near each of the corners to induce a
122 consistent current. The pumps were configured to draw water from their base and then propel it outward
123 parallel to the bottom of the pool. The pumps were oriented successively at right angles to one another,
124 which created a counterclockwise circulation of 2-3 cm s⁻¹ (Else et al., 2015).

125 Bulk ice and seawater temperatures were recorded by an automated type-T thermocouple array fixed
126 vertically in the pool. Seawater salinity was measured continuously using Aanderaa CT sensors (model
127 4319) located at 30, 100, 175 and 245 cm depth. The in situ seawater *p*CO₂ was measured every 5 sec
128 using a Contros HydroC (resolution < 1 μ atm, accuracy \pm 1% of the upper range value) located at 1.3 m
129 depth.

130 Air temperature and relative humidity were measured using a Vaisala HMP45C probe at a
131 meteorological station located 2 m above the sea ice surface. Solar irradiance was continuously recorded
132 by an Eppley Precision Spectral Pyranometer (range=0.285–2.8 μ m) mounted 10 m above the sea ice
133 surface. In addition, estimated photosynthetically active radiation (PAR) values at the ice bottom were
134 recorded with Alec mkv-L PAR sensors throughout the study and ranged from 0 to 892 μ mol photons m⁻²
135 s⁻¹.

136 Sea ice and seawater samples were obtained from a confined area located on the North side of the
137 pool to minimize effects on other experiments (e.g. Else et al., 2015). Ice samples were collected using
138 ceramic knives or a Kovacs Mark II coring system depending on the ice thickness. Sampling was
139 performed from a movable bridge to avoid walking on the ice surface and to ensure only undisturbed sites
140 were sampled. Ice cores were collected from one end of the pool (half meter away from the edge of the
141 pool) and at least 20 cm away from previous cored sites. Ice cores were packed in clean plastic bags and
142 kept frozen during the 20 minutes transport to a cold laboratory and processed within a few hours.
143 Seawater was sampled for total alkalinity (TA) and total dissolved inorganic carbon (TCO₂) with a
144 peristaltic pump (Cole Palmer, Masterflex-Environment sampler, equipped with PTFE tubing) through an
145 ice core hole the ice-water interface, at 1.25 m, and 2.5 m depth. Samples were stored in 12 ml gas-tight

146 vials (Exetainer, Labco High Wycombe, UK) and poisoned with 12 μl of saturated HgCl_2 solution and
147 stored in the dark at 4°C until analysed.

148 Air-ice CO_2 fluxes were measured using a Li-Cor 8100-103 chamber associated with a LI-8100A soil
149 CO_2 flux systems. The chamber was connected in a closed loop to the IRGA with an air pump rate of 3 L
150 min^{-1} . The measurement of $p\text{CO}_2$ in the chamber was recorded every sec over a 15 minute period. The
151 flux was computed from the slope of the linear regression of $p\text{CO}_2$ against time ($r^2 > 0.99$) according to
152 Frankignoulle (1988), taking into account the volume of ice or snow enclosed within the chamber. The
153 uncertainty of the flux computation due to the standard error on the regression slope was on average $\pm 3\%$.

154 In the cold laboratory, sea ice cores were cut into 2 cm sections using a pre-cleaned stainless steel
155 band saw. Each section was placed in a gas-tight laminated (Nylon, ethylene vinyl alcohol and
156 polyethylene) plastic bag (Hansen et al., 2000) fitted with a gastight Tygon tube and a valve for sampling.
157 The plastic bag was sealed immediately and excess air was gently removed through the valve using a
158 vacuum pump. The bagged sea ice samples were then melted in the dark at 4°C to minimize the
159 dissolution of calcium carbonate precipitates (meltwater temperature never rose significantly above 0°C).
160 Once melted, the meltwater mixture and bubbles were transferred to gas-tight vials (12 ml Exetainer,
161 Labco High Wycombe, UK), poisoned with 12 μl solution of saturated HgCl_2 and stored in the dark at
162 4°C until analysed.

163 Bulk ice and seawater salinities were measured using a Thermo Orion 3-star with an Orion
164 013610MD conductivity cell and values were converted to bulk salinity (Grasshoff et al., 1983). TA was
165 determined by potentiometric titration (Haraldsson et al., 1997) while TCO_2 was measured on a
166 coulometer (Johnson et al., 1987). Routine analysis of Certified Reference Materials provided by A. G.
167 Dickson, Scripps Institution of Oceanography, verified that TA and TCO_2 were analyzed within ± 3 and
168 $\pm 2 \mu\text{mol kg}^{-1}$, respectively. Brine volume was estimated from measurements of bulk salinity, temperature
169 and density according to Cox and Weeks (1983) for temperatures below -2°C and according to
170 Leppäranta and Manninen (1988) for ice temperatures within the range -2 to 0°C.

171 Bulk ice samples for biological measurements were collected between 14 and 21 January. Filtered
172 (0.2 μm) SERF seawater (FSW) was added at a ratio of 3 parts FSW to 1 part ice and the samples were
173 left to melt in the dark. Chlorophyll *a* was determined on three occasions by filtering two aliquots of the
174 melted ice sample onto GF/F filters (Whatmann brand) and extracting pigments in 10 ml of 90% acetone

175 for 24 h. Fluorescence was measured before and after the addition of 5% HCl (Turner Designs
176 Fluorometer) and Chl *a* concentration was calculated following Parsons et al. (1984). Measurements of
177 bacterial production were done four times during the biological sampling period by incubating 6-10 ml
178 subsamples of the ice-FSW solution with ^3H -leucine (final concentration of 10 nM) for 3h at 0°C in
179 darkness (Kirchmann, 2001). Half of the samples were spiked with trichloroacetic acid (TCA, final
180 concentration 5%) as controls prior to the incubation, while the remaining active subsamples were fixed
181 with TCA (final concentration 5%) after incubation. Following the incubation, vials were placed in 80°C
182 water for 15 minutes (Garneau et al., 2006) before filtration through 0.2 μm cellulose acetate membranes
183 (Whatmann brand) and rinsing with 5% TCA and 95% ethanol. Filters were dried and dissolved in
184 scintillation vials by adding 1 ml ethyl acetate, and radioactivity was measured on a liquid scintillation
185 counter after an extraction period of 24 h. Bacterial production was calculated using the equations of
186 Kirchman (1993) and a conversion factor of 1.5 kg C mol $^{-1}$ (Ducklow et al., 2003).

187 **4. Results**

188 **4.1. Sea ice and seawater physical conditions**

189 Sea ice was grown in the pool from open water on 13 January 2013 and reached a maximum thickness
190 of 24 cm on 26 January at which point the heat at the base of the pool was turned on. On 30 January the
191 experiment ended with the pool 20% ice-free. Three main snowfall events occurred during the
192 experiment. The first, from 14 to 15 January, covered the sea ice surface with 1 cm of snow. The second,
193 from 18 to 23 January, deposited 6-9 cm of snow over the entire pool. On the morning of 23 January, the
194 snow was manually cleared off the ice surface to investigate the insulating effect of the snow on the ice
195 temperature and ikaite precipitation (Rysgaard et al., 2014). Finally, from noon on 24 January to 27
196 January, 8 cm of snow covered the entire pool until the end of the experiment on 30 January.

197 The air temperature at the beginning of the experiment ranged from -2°C to -26°C, which initiated
198 rapid sea ice growth to 15 cm until 18 January (Fig. 2). During this initial sea ice growth, the sea ice was
199 attached to the side of the pool resulting in the development of a hydrostatic pressure head that caused
200 percolation of seawater at the freezing point upwards through the sea ice volume as the sea ice grew
201 downwards. This resulted in repeated events of increased sea ice temperature from the bottom to the
202 surface observed between 15 and 18 January (Fig. 2). Subsequently, the ice was cut using an ice saw
203 around the perimeter, allowing the ice to float and a pressure release valve was installed to prevent such

204 events (Rysgaard et al., 2014). During this period, the ice temperature oscillated between relatively warm
205 (~ -3°C) and cold (~ -7°C) phases. Brine volume content (0.047) was low in the middle part of the ice
206 cover, close to the permeability threshold of 0.05 as suggested by Golden et al., (2007). The bulk ice
207 salinity profiles were typically C-shaped with values ranging from 6 to 23 (Fig. 2). The underlying
208 seawater salinity increased rapidly due to sea ice growth. From 18 to 23 January, the 9 cm snow cover
209 insulated the ice cover from the cold atmosphere (Rysgaard et al., 2014), resulting in a fairly constant ice
210 thickness, nearly no change in ice temperature and salinity, a brine volume content above the
211 permeability threshold and a small increase in the underlying seawater salinity. Once the ice surface was
212 cleared of snow on the morning of 23 January, the ice temperature decreased throughout the entire ice
213 thickness and the ice surface salinity increased. The sea ice volume cooled from the top downwards, and
214 the brine volume content decreased below the permeability threshold on 23 January and rapid sea ice
215 growth rapidly increased the seawater salinity. Shortly after the snow clearing, the last snowfall event
216 covered the ice surface with 8 cm of snow, reducing the effect of the cold atmosphere on the ice cover.
217 On 26 January, the heater was activated to initiate sea ice melt. Sea ice temperatures increased and
218 became isothermal around -2°C while the bulk ice salinity decreased and the brine volume content
219 increased up to 0.13. The sea ice melt decreased the seawater salinity. The pool was well mixed during
220 the whole growth phase with similar salinity and temperature observed at the four depths. However, once
221 the heat was turned on, the pool became stratified with respect to salinity changes, as the salinity at 30 cm
222 depth started to diverge from the deeper depths (Fig. 2).

223 4.2. Carbonate system

224 TA and TCO_2 in seawater, noted as $TA_{(sw)}$ and $TCO_{2(sw)}$, were sampled at the sea ice-seawater
225 interface, 1.25 and 2.5 m depth. An ANOVA test over the 3 depths revealed that the means are not
226 statistically different ($p<0.01$) so we consider the average concentration of the three depths in the
227 following analysis. During sea ice growth, $TA_{(sw)}$ increased from 2449 to 2644 $\mu\text{mol kg}^{-1}$ (black line, Fig.
228 3a) while $TCO_{2(sw)}$ increased from 2347 to 2516 $\mu\text{mol kg}^{-1}$ (black line, Fig. 3b). Once the ice started to
229 melt, $TA_{(sw)}$ decreased to 2607 $\mu\text{mol kg}^{-1}$ and $TCO_{2(sw)}$ decreased to 2461 $\mu\text{mol kg}^{-1}$. As the experiment
230 stopped before the ice was completely melted in the tank, both the seawater salinity and $TA_{(sw)}$ do not
231 reach their initial values at the end of the experiment (Table 1, Fig 2 and 3). To discard the effect of
232 salinity changes, we normalized $TA_{(sw)}$ and $TCO_{2(sw)}$ to a salinity of 33 (noted as $nTA_{(sw)}$ and $nTCO_{2(sw)}$)
233 according to the equations 4 and 5:

234 $nTA_{(sample) t} = \frac{TA_{(sample) t}}{S_{(sample) t}} \times 33$ (4)

235 $nTCO_{2 (sample) t} = \frac{TCO_{2 (sample) t}}{S_{(sample) t}} \times 33$ (5)

236 where t is the time of the sampling and S the salinity of the sample (seawater or sea ice). During ice
 237 growth, $nTA_{(sw)}$ and $nTCO_{2(sw)}$ increased slightly to 2446 and 2328 $\mu\text{mol kg}^{-1}$, respectively (Fig. 3c).
 238 However, once the ice started to melt, $nTA_{(sw)}$ increased to 2546 $\mu\text{mol kg}^{-1}$ and $nTCO_{2(sw)}$ increased to
 239 2404 $\mu\text{mol kg}^{-1}$.

240 The in situ $p\text{CO}_2$ of the underlying seawater ($p\text{CO}_{2(sw)}$) decreased from 377 to 360 μatm as the
 241 seawater temperature in the pool decreased to the freezing point. The $p\text{CO}_{2(sw)}$ then oscillated from 360 to
 242 365 μatm during sea ice growth. One day after the heater was turned on, the $p\text{CO}_{2(sw)}$ increased to a
 243 similar concentration as at the beginning of the experiment before decreasing to 373 μatm by the end of
 244 the experiment (Fig. 3d).

245 Within bulk sea ice, $TA_{(ice)}$ ranged from 300 to 1907 $\mu\text{mol kg}^{-1}$ while $TCO_{2(ice)}$ ranged from 237 to
 246 1685 $\mu\text{mol kg}^{-1}$. Both $TA_{(ice)}$ and $TCO_{2(ice)}$ exhibited C-shaped profiles with higher concentrations at the
 247 surface and bottom layers of the ice cover (Fig. 4). The concentration of $TA_{(ice)}$ (average = 476 $\mu\text{mol kg}^{-1}$)
 248 and $TCO_{2(ice)}$ (average = 408 $\mu\text{mol kg}^{-1}$) did not show significant variability during our survey, except at
 249 the surface of the ice. A first maximum was observed on 17 January with concentration of 1907 $\mu\text{mol kg}^{-1}$
 250 for TA and 1685 $\mu\text{mol kg}^{-1}$ for TCO_2 . A second maximum was observed on 23 January with
 251 concentration of 1433 $\mu\text{mol kg}^{-1}$ for TA and 861 $\mu\text{mol kg}^{-1}$ for TCO_2 . These maxima matched the high
 252 bulk ice salinity (Fig. 2), so we also normalized $TA_{(ice)}$ and $TCO_{2(ice)}$ (noted as $nTA_{(ice)}$ and $nTCO_{2(ice)}$, Fig.
 253 4) to a salinity of 33 (according to the equations 4 and 5) to discard the effect of salinity changes and
 254 facilitate comparison with the underlying seawater. During initial sea ice formation (up to 17 January),
 255 the concentration of both $nTA_{(ice)}$ (from 1083 to 2741, average = 1939 $\mu\text{mol kg}^{-1}$) and $nTCO_{2(ice)}$ (from
 256 853 to 2440, average = 1596 $\mu\text{mol kg}^{-1}$) were at their minima in the experimental time series. From 17 to
 257 21 January, both $nTA_{(ice)}$ and $nTCO_{2(ice)}$ increased throughout the ice column (average $nTA_{(ice)} = 2375$
 258 $\mu\text{mol kg}^{-1}$ and $nTCO_{2(ice)} = 2117 \mu\text{mol kg}^{-1}$). However, from 21 January until the initial sea ice melt,
 259 $nTA_{(ice)}$ and $nTCO_{2(ice)}$ decreased in the top 5 cm of the ice cover (average $nTA_{(ice)} = 2125 \mu\text{mol kg}^{-1}$ and
 260 $nTCO_{2(ice)} = 1635 \mu\text{mol kg}^{-1}$).

261 **4.3. Air-ice CO_2 fluxes**

262 The CO₂ fluxes measured at the variably snow-covered sea ice surface (Fig. 2b), ranged from 0.29 to
263 4.43 mmol m⁻² d⁻¹ show that growing sea ice released CO₂ to the atmosphere (Fig. 5). However, as soon
264 as the ice started to warm up and then melt, the sea ice switched from source to sink for atmospheric CO₂
265 with downward fluxes from -1.3 to -2.8 mmol m⁻² d⁻¹. These ranges of air-ice CO₂ exchanges are of the
266 same order of magnitude as fluxes reported on natural sea ice using the same chamber technique in the
267 Arctic during the initial sea ice growth (from 4.2 to 9.9 mmol m⁻² d⁻¹ in Geilfus et al., 2013) and during
268 the spring-summer transition (from -1.4 to -5.4 mmol m⁻² d⁻¹ in Geilfus et al., 2015). In Antarctica air-ice
269 CO₂ fluxes were reported during the spring-summer transition from 1.9 to -5.2 mmol m⁻² d⁻¹ by Delille et
270 al (2014), from 0.3 to -2.9 mmol m⁻² d⁻¹ (Geilfus et al., 2014) and from 0.5 to -4 mmol m⁻² d⁻¹ (Nomura et
271 al., 2013).

272 5. Discussion

273 5.1. Key processes affecting the carbonate system

274 The dynamics of inorganic carbon in the ocean and sea ice are mainly affected by temperature and
275 salinity changes, precipitation and dissolution of calcium carbonate, and biological activities (Zeebe and
276 Wolf-Gladrow, 2001). During this experiment, neither organic matter nor biota were purposely
277 introduced into the pool; the observed range of bulk ice microbial activity (5.7×10^{-9} on 14 January to 7.5
278 $\times 10^{-7}$ g C L⁻¹ h⁻¹ on 21 January) and algal Chl *a* (0.008 on 14 January to 0.002 $\mu\text{g L}^{-1}$ on 21 January) were
279 too low to support any biological activity (Rysgaard et al., 2014). Therefore biological activity is unlikely
280 to have played a role. During the same 2013 time series at SERF, Rysgaard et al. (2014) discussed the
281 precipitation of ikaite within the ice cover in detail, reporting high concentrations of ikaite ($> 2000 \mu\text{mol}$
282 kg^{-1}) at the surface of the ice in brine skim and frost flowers and ikaite precipitation up to $350 \mu\text{mol kg}^{-1}$
283 within bulk sea ice. Within sea ice, ikaite precipitation is associated with low ice temperatures, high bulk
284 salinity and high TA_(ice) and TCO_{2(ice)} concentrations (Fig. 2 and 3).

285 The main processes affecting the carbonate system can be described by changes in TA and TCO₂
286 (Zeebe and Wolf-Gladrow, 2001). An exchange of CO_{2(gas)} affects TCO₂ while TA remains constant and
287 the precipitation-dissolution of calcium carbonate affects both TA and TCO₂ in a ratio of 2:1 (see
288 equation 1 to 3, Fig. 6). To calculate the theoretical changes in TA and TCO₂ during the course of the
289 experiment, we used seawater samples from 11 January prior to sea ice formation (t=0, Table 1) as the
290 origin point (blue circle on Fig. 6). Sea ice data are located between the theoretical calcium carbonate
291 precipitation line and the CO₂ release line (Fig. 6a) while seawater data mainly fall on the calcium

292 carbonate dissolution line (Fig. 6b), suggesting that the carbonate system within sea ice is affected by
293 both the precipitation of ikaite and a release of $\text{CO}_{2(\text{gas})}$ while the underlying seawater is mainly affected
294 by the dissolution of calcium carbonate.

295 **5.2. Estimation of the precipitation-dissolution of ikaite**

296 During the experiment, Rysgaard et al., (2014) observed ikaite within sea ice using direct microscopic
297 observations. The precipitation-dissolution of ikaite and gas exchange are the only two processes taking
298 place during the experiment. As illustrated in Fig. 6, an exchange of CO_2 does not affect TA while the
299 precipitation-dissolution of ikaite affects TA and TCO_2 in a ratio 2:1. Therefore, we use TA to estimate
300 how much ikaite is precipitated or dissolved within the ice cover and the underlying seawater.

301 Assuming no biological effect, ikaite precipitation/dissolution and gas exchange, TA and TCO_2 are
302 considered conservative with salinity. Therefore, we can calculate the expected TA and TCO_2 (noted as
303 $\text{TA}_{(\text{ice})}^*$ and $\text{TCO}_{2(\text{ice})}^*$ in the ice cover and $\text{TA}_{(\text{sw})}^*$, $\text{TCO}_{2(\text{sw})}^*$ for the water column) based on the initial
304 seawater conditions ($\text{TA}_{(\text{sw})}$, $\text{TCO}_{2(\text{sw})}$ and $\text{S}_{(\text{sw})}$ at $t=0$, Table 1) and the sample salinity (bulk sea ice or
305 seawater) measured during the experiment:

$$306 \text{TA}_{(\text{sample})}^* t = \frac{\text{TA}_{(\text{sw})} t=0}{\text{S}_{(\text{sw})} t=0} \times \text{S}_{(\text{sample})} t \quad (6)$$

$$307 \text{TCO}_{2(\text{sample})}^* t = \frac{\text{TCO}_{2(\text{sw})} t=0}{\text{S}_{(\text{sw})} t=0} \times \text{S}_{(\text{sample})} t \quad (7)$$

308 where t is the time of the sampling. Within the ice cover, $\text{TA}_{(\text{ice})}$, $\text{TCO}_{2(\text{ice})}$, and the bulk ice salinity are
309 averaged throughout the ice column at each sampling day (Fig. 7a, b, black line) while for the underlying
310 seawater, we used the averaged $\text{TA}_{(\text{sw})}$, $\text{TCO}_{2(\text{sw})}$ and salinity for all the measured depths (Fig. 2a, b, black
311 line). The difference between $\text{TA}_{(\text{sample})}^*$ and the observed TA is only due to the precipitation or
312 dissolution of ikaite crystals. In case of ikaite precipitation (*i.e.* $\text{TA}_{(\text{sample})}^* > \text{TA}_{(\text{sample})}$), half of this
313 positive difference corresponds to the amount of ikaite precipitated within the ice. This ikaite may either
314 remain or may be exported out of the ice. A negative difference (*i.e.* $\text{TA}_{(\text{sample})}^* < \text{TA}_{(\text{sample})}$), indicates
315 ikaite dissolution.

316 **5.2.1. Sea ice**

317 Greater $\text{TA}_{(\text{ice})}^*$ and $\text{TCO}_{2(\text{ice})}^*$ compared to the averaged observed $\text{TA}_{(\text{ice})}$ and $\text{TCO}_{2(\text{ice})}$ (Fig. 7a, b) are
318 expected as ikaite is precipitated and CO_2 released from the ice to the atmosphere (Fig. 5, 6). Half the
319 difference between $\text{TA}_{(\text{ice})}^*$ and $\text{TA}_{(\text{ice})}$ is a result of ikaite precipitation (Fig. 7c, black diamonds). Highly

variable ikaite precipitation was observed (Fig. 7c). Ikaite precipitation was up to $167 \mu\text{mol kg}^{-1}$ (e.g. first days of the experiment) and as low as $1 \mu\text{mol kg}^{-1}$ (e.g. 19 January). A negative difference between $\text{TA}_{(\text{ice})}^*$ and $\text{TA}_{(\text{ice})}$ (*i.e.* ikaite dissolution) occurred on three occasions: 14, 20 and after the 26 January (beginning of the sea ice melt). On these occasions, the ice cover was relatively warm due to warmer atmospheric temperatures (14 January), thicker snow cover insulating the ice cover from the cold atmosphere (20 January) or when heat was turned back on (after 26 January, Fig. 2). Relatively high sea ice temperatures likely promote ikaite dissolution in agreement with Rysgaard et al., (2014) who linked ikaite precipitation/dissolution to ice temperature. The upward percolation of seawater observed from 15 to 18 January might complicate the effect of sea ice temperature on ikaite formation because it was in part responsible for increased ice temperatures (Fig. 2b) and therefore increased the sea ice brine volumes (Fig. 2c). Increased vertical connectivity (permeability) of the network of liquid inclusions throughout the sea ice (Golden et al., 2007; Galley et al., 2015) would have allowed the export of ikaite crystals from the ice cover to the underlying seawater. However, while we calculated a negative difference between $\text{TA}_{(\text{ice})}^*$ and $\text{TA}_{(\text{ice})}$, ikaite crystals were observed by Rysgaard et al., (2014). We compared the direct microscopy observations by averaging the amount of ikaite precipitated throughout the ice thickness for each sampling day from Rysgaard et al., (2014) (Fig. 7c, white dots) with our estimation of the amount of ikaite based on the difference between $\text{TA}_{(\text{ice})}^*$ and $\text{TA}_{(\text{ice})}$ (Fig. 7c, black diamonds). Both ikaite measurements are of the same order of magnitude however the average ($22 \mu\text{mol kg}^{-1}$) and maximum ($100 \mu\text{mol kg}^{-1}$) of direct observations presented by Rysgaard et al. (2014) were lower than our estimated average ($40 \mu\text{mol kg}^{-1}$) and maximum of up to $167 \mu\text{mol kg}^{-1}$ over this whole experiment. Deviations are likely due to methodological differences. Here, sea ice samples were melted to subsample for TA and TCO_2 . Ikaite crystals may have dissolved during melting, leading to an underestimation of the total amount of ikaite precipitated in the ice. However, the difference between $\text{TA}_{(\text{ice})}^*$ and $\text{TA}_{(\text{ice})}$ provides an estimation of how much ikaite is precipitated in the ice cover, including those crystals potentially already exported to the underlying seawater. The method used by Rysgaard et al., (2014) avoid the bias of ikaite dissolution during sea ice melt with the caveat that crystals need to be large enough to be optically detected. If no crystals were observed, Rysgaard et al., (2014) assumed that no crystals were precipitated in the ice, though ikaite crystals could have been formed and then exported into the underlying seawater prior to microscopic observation of the sample, which may explain the difference observed between both methods during initial sea ice formation (15-18 January) when the ice was still very thin. In addition, the

350 succession of upward percolation events could have facilitated the ikaite export from the ice cover to the
351 underlying seawater. Estimations from both methods show similar concentrations when the ice (i)
352 warmed due to snowfall (18-23 January) and (ii) cooled once the snow was removed (on 23 January).
353 Once the ice started to melt (26 January), Rysgaard et al., (2014) reported a decrease in the ikaite
354 precipitation while in this study we reported a negative difference between $TA_{(ice)}^*$ and $TA_{(ice)}$, possibly
355 indicating that ikaite dissolved in the ice.

356 **5.2.2. Water column**

357 The main process affecting the carbonate system in the underlying seawater in this study is the export
358 of ikaite from the ice and its dissolution in the water column (Fig. 6). While a few studies of ikaite
359 precipitation within sea ice carried out over open ocean hypothesized that ikaite remained trapped within
360 the sea ice matrix (Rysgaard et al., 2007; 2013; Delille et al., 2014), the observed increase of $nTA_{(sw)}$ (Fig.
361 3) suggests that ikaite precipitated within the ice cover was exported to the underlying seawater where the
362 crystals were dissolved as suggested by Fransson et al., (2013). Lower $TA_{(sw)}^*$ and $TCO_{2(sw)}^*$ compared to
363 $TA_{(sw)}$ and $TCO_{2(sw)}$ (Fig. 3) confirm the dissolution of ikaite in the underlying seawater as the dissolution
364 of ikaite crystals will decrease both TA and TCO_2 (equations 1 to 3). Therefore, half the difference
365 between $TA_{(sw)}^*$ and $TA_{(sw)}$ corresponds to the concentration of ikaite exported from the ice and dissolved
366 in the underlying seawater (Fig. 8a). This concentration increased over time to a maximum of 66 μmol
367 kg^{-1} .

368 During this experiment, $nTA_{(sw)}$ increased by 128 $\mu\text{mol kg}^{-1}$ while $nTCO_{2(sw)}$ increased by 82 $\mu\text{mol kg}^{-1}$
369 (Fig. 3c). This suggests that 64 $\mu\text{mol kg}^{-1}$ of ikaite are dissolved compared to the 66 $\mu\text{mol kg}^{-1}$ estimated
370 from the difference between $TA_{(sw)}^*$ and $TA_{(sw)}$. As a result of the effect of ikaite dissolution on the 2:1
371 ratio of TA: TCO_2 , the dissolution of ikaite accounts for the entire increase of $nTA_{(sw)}$ but only accounts
372 for 64-66 $\mu\text{mol kg}^{-1}$ of the 82 $\mu\text{mol kg}^{-1}$ increase in $nTCO_{2(sw)}$. So, 16-18 $\mu\text{mol kg}^{-1}$ (about 25%) of the
373 increase of $nTCO_{2(sw)}$ cannot be explained by the dissolution of ikaite. The increase of both $nTA_{(sw)}$ and
374 $nTCO_{2(sw)}$ is more significant once the ice starts to melt (26 January). During sea ice melt, increased
375 vertical permeability resulting in increased liquid communication through the sea ice volume from below
376 likely in part dissolved ikaite crystals still residing in the ice at that time, and also will have created a
377 downward crystal export mechanism. As the ice melt advanced, patches of open water occurred at the
378 surface of the pool. Therefore, uptake of atmospheric CO_2 by the undersaturated seawater likely occurred,
379 increasing the $TCO_{2(sw)}$.

The dissolution of ikaite crystals could also have a strong impact on the $p\text{CO}_{2(\text{sw})}$. The water column was undersaturated compared to the atmosphere during the whole experiment (Fig. 3d). A release of CO_2 , from the ice to the atmosphere was measured during sea ice growth (Fig. 5) in spite of the undersaturated $p\text{CO}_{2(\text{sw})}$. This suggests that air-ice CO_2 fluxes are only due to the concentration gradient between the ice and the atmosphere (Geilfus et al., 2012; Nomura et al., 2013) but that sea ice exchanges CO_2 with the atmosphere independently of the seawater concentration (Geilfus et al., 2014). The $p\text{CO}_{2(\text{sw})}$ is highly correlated with the seawater temperature (Fig. 2) with a rapid decrease of $p\text{CO}_{2(\text{sw})}$ during the first days of the experiment (13 to 15 January) and a relative constant $p\text{CO}_{2(\text{sw})}$ until 27 January. However, on 26 January, the heat was turned back on affecting the seawater temperature on the same day (Fig. 2) while the impact of increasing temperature on the $p\text{CO}_{2(\text{sw})}$ appeared one day later (Fig. 3d). We normalized the $p\text{CO}_{2(\text{sw})}$ to a temperature of -1°C (after Copin-Montegut (1988), noted as $np\text{CO}_{2(\text{sw})}$, blue line on Fig. 3d). The $np\text{CO}_{2(\text{sw})}$, does not show major variations during sea ice growth with values around $380 \mu\text{atm}$. However, once the heat is turned on and the seawater temperature increased (on 26 January), $np\text{CO}_{2(\text{sw})}$ decreased from $383 \mu\text{atm}$ to $365 \mu\text{atm}$, while $p\text{CO}_{2(\text{sw})}$ did not change in response to increased seawater temperatures until 27 January, suggesting that a process other than temperature change affected the $p\text{CO}_{2(\text{sw})}$. According to equation 1, the dissolution of calcium carbonate has the potential to reduce $p\text{CO}_{2(\text{sw})}$. Therefore, during sea ice growth and the associated release of salt, TA, TCO_2 and ikaite crystals to the underlying seawater, ikaite dissolution within the seawater could be responsible for maintaining stable $p\text{CO}_{2(\text{sw})}$ values while seawater salinity, $\text{TA}_{(\text{sw})}$ and $\text{TCO}_{2(\text{sw})}$ are increasing. Once the seawater temperature increased (26 January), sea ice melt likely released ikaite crystals to the underlying seawater (Fig. 2, 8a) along with brine and meltwater, a process that would continuously export ikaite from the sea ice as the volume interacting with the seawater via percolation or convection increased. The dissolution of these crystals likely contributed to keeping the $p\text{CO}_{2(\text{sw})}$ low and counterbalancing the effect of increased temperature. We argued that once all the ikaite crystals are dissolved, the increase seawater temperature increased the $p\text{CO}_{2(\text{sw})}$ simultaneously with the $np\text{CO}_{2(\text{sw})}$ (27 January, Fig. 3).

5.3. Ikaite export from the ice cover to the water column

We estimated the amount of ikaite precipitated and dissolved within sea ice and seawater based on the sea ice (and seawater) volume (in m^3), the sea ice and seawater density, the concentration of ikaite precipitated and dissolved within the ice cover (Fig. 7c), and the concentration of ikaite dissolved in the water column (Fig. 8a). Within the ice cover, the amount of ikaite precipitated-dissolved ranged from -0.7

410 to 1.97 mol (Fig 8b, Table 2), with a maximum just after the snow was cleared on 23 January. In the
411 underlying seawater, the amount of ikaite dissolved in the pool increased from 0.47 mol on the first day
412 of the experiment to 11.5 mol on 25 January when sea ice growth ceased. Once the ice started to melt the
413 amount of dissolved ikaite increased up to 20.9 (28 Jan) and 26.7 mol (29 January, Table 2). The
414 estimation of ikaite dissolution in the pool is significantly higher than the estimated amount of ikaite
415 precipitated (and potentially exported) within the ice cover, especially during sea ice melt. Within the ice
416 cover, the ikaite values presented here represent a snapshot of the ikaite content in the ice at the time of
417 sampling. In the underlying seawater, ikaite dissolution increased $TA_{(sw)}$ cumulatively over time.

418 The difference between $TA_{(ice)}^*$ and $TA_{(ice)}$ provides an estimation of ikaite precipitated within the ice,
419 including potential ikaite export to the underlying seawater, so it cannot be used to determine how much
420 ikaite remained in the ice versus how much dissolved in the water column. However, Rysgaard et al.,
421 (2014) indicate ikaite precipitated within the ice based on direct observations. Using the ikaite
422 concentration reported in Rysgaard et al (2014) (and shown in Fig. 7c), the sea ice volume (in m^3) and
423 density, we calculate that 0 to 3.05 mol of ikaite precipitated within the ice cover during sea ice growth
424 (Fig. 8b and Table 2). This amount decreased to 0.46 and 0.55 mol during the sea ice melt (28 and 29
425 January, respectively). Increased ikaite dissolution in the water column when the ice began to melt (from
426 11.5 to 20.9 mol) indicates that 9.4 mol of ikaite were stored in the ice and rejected upon the sea ice melt.
427 This amount is about three times the amount of ikaite precipitated in the ice estimated by Rysgaard et al.,
428 (2014) at the end of the growth phase (3.05 mol, Table 2), suggesting more work is needed best estimate
429 ikaite precipitation within sea ice.

430 Once the ice started to melt, the increased ikaite dissolution from 11.5 mol to 20.9 mol (28 January) and
431 to 26.7 mol (29 January) suggests that about the same amount of ikaite is dissolved during the sea ice
432 growth as during the first two days of the sea ice melt. The amount of ikaite dissolved in the water
433 column after melt commenced continued to increase cumulatively, suggesting that ikaite is continuously
434 exported to the underlying seawater as increased sea ice temperatures permit more of the volume to
435 communicate with the underlying seawater. Therefore, we can assume than more than half of the amount
436 of ikaite precipitated within the ice remained in the ice cover before ice melt began.

437 **5.4. Air-ice-seawater exchange of inorganic carbon**

438 SERF is a semi-closed system where the only way for the surface (water or sea ice) to gain or lose CO₂
439 is through exchange with the atmosphere, making it reasonable to track the exchange of TCO₂ in the
440 atmosphere-sea ice-seawater system. The ice cover always had lower TCO_{2(ice)} during the experiment
441 (TCO_{2(ice)}^{*} > TCO_{2(ice)}) compared to what would be expected if the CO₂ simply followed brine rejection in
442 a conservative process (i.e. TCO_{2(ice)}^{*}) (Fig. 7b). This could be due to: (i) CO₂ released to the atmosphere
443 from sea ice, (ii) decreased TCO_{2(ice)} due to the precipitation of ikaite within sea ice and/or (iii) sea ice
444 exchanging TCO₂ with the underlying seawater.

445 The number of moles of TCO₂ exchanged during this experiment was calculated using the sea ice (and
446 seawater) volume (in m³) and density (in kg/m³). The total amount of TCO_{2(ice)} lost from the ice cover (the
447 difference between TCO_{2(ice)}^{*} and TCO_{2(ice)}) ranged from 0.11 to 6.02 mol (average 2.38 mol, Fig. 9, black
448 dots). The greatest sea ice TCO₂ losses occurred on 15-16 January during initial sea ice growth and from
449 23 to 25 January, during ice cooling due to snow removal. The exchange of CO₂ between the ice and the
450 atmosphere is known (Fig. 5). The number of mole of CO₂ exchanges between the ice and the atmosphere
451 were calculated (noted as CO_{2(air-ice)} in Table 2) using the time step between each flux measurement, the
452 ice thickness and density. During sea ice growth 0.01 to 0.42 mol of CO₂ were released from the ice-
453 covered pool to the atmosphere. During sea ice melt uptake of atmospheric CO₂ by the ice-covered pool
454 ranged from -0.15 to -0.93 (Fig. 9, white triangles). On average, over the duration of the experiment, the
455 ice cover released 0.08 mol of CO₂ to the atmosphere. Assuming we know how much ikaite is contained
456 within the ice cover (Fig. 8b), we can estimate how much TCO₂ is exported from the ice to the underlying
457 seawater (Fig. 9, blue triangles) by subtracting the air-ice CO₂ exchange and the ikaite precipitation from
458 the total reduction of TCO_{2(ice)} observed within the ice cover (Fig. 9, black dots). The sea ice-to-seawater
459 TCO₂ export ranged from 0.2 to 3.98 mol (average = 1.7 mol), confirming that sea ice primarily exports
460 TCO₂ to the underlying seawater. TCO₂ export from the ice to the water column ranged from 23% of the
461 total sea ice TCO₂ early in the ice growth (14 January) to 100% after the onset of melt. These estimations
462 are comparable to the study of Sejr et al., (2011) who suggested that sea ice exports 99% of its total TCO₂
463 to the seawater below it. On average over the whole experiment, sea ice exported 1.7 mol of TCO₂ to the
464 underlying seawater (Fig. 9), which corresponds to a TCO_{2(sw)} increase of 43.5 μmol kg⁻¹ considering the
465 average sea ice thickness and density during the experiment and the volume of the pool. However,
466 TCO_{2(sw)} increased by 115 μmol kg⁻¹ over the whole experiment (Fig. 3b), leaving an increase of 71.5
467 μmol kg⁻¹ in the TCO_{2(sw)} that cannot be explained by the sea ice-seawater exchange of TCO₂. We

468 postulate that as the ice melt advanced, patches of open water that opened at the surface of the pool which
469 were undersaturated compared to the atmosphere (Fig. 3d) imported the additional TCO_2 directly from the
470 atmosphere in the form of $CO_{2(g)}$. Considering the pool volume, the $71.5 \mu\text{mol kg}^{-1}$ increase of $TCO_{2(sw)}$
471 could be explained by an air-sea water CO_2 uptake of $8.5 \text{ mmol m}^{-2} \text{ d}^{-1}$ over 3 days of sea ice melt in a
472 20% ice free pool. High air-sea gas exchanges rates have been observed over partially ice-covered seas
473 (Else et al., 2011; 2013). This mechanism is also corroborated by models that account for additional
474 sources of turbulence generated by the presence of sea ice (Loose et al., 2014).

475 The design of the experiment allowed for constrained measurements of inorganic carbon fluxes
476 between sea ice and the water column not possible in a natural environment where large volume, mixing
477 processes alter the underlying seawater making it more complicated to identify changes. We build a CO_2
478 budget based only on the sea ice growth phase because only two days of data for the melt phase are
479 available and the experiment stopped while the pool was 20% ice-free (Rysgaard et al., 2014; Else et al.,
480 2015). The initial seawater (origin point, $t=0$) contained 1040.9 mol of $TCO_{2(sw)}$ on 11 January while on
481 the last day of sea ice growth (25 January) the seawater contained 1017.3 mol of $TCO_{2(sw)}$ (Table 2) with
482 the difference, (23.6 mol of TCO_2) in all likelihood transferred from the water column to the ice cover or
483 the atmosphere. However, the TCO_2 content within the ice cover at the end of the growing phase was 15.6
484 mol and the ice cover released 3.1 mol of CO_2 to the atmosphere (Table 2). Therefore, 4.9 mol of the 23.6
485 mol of TCO_2 exchanged from the water column are unaccounted for, but may be explained by air-ice CO_2
486 fluxes. The chamber measurement technique for air-ice CO_2 flux may underestimate the exchange of
487 CO_2 , and the air-seawater CO_2 fluxes are unknown until the ice started to grow (13 January). These
488 missing moles of TCO_2 may also be explained by our assumption of uniform sea ice thickness in the
489 SERF. Using the seawater conditions at the end of the experiment, 1-cm of seawater in the pool contains
490 4.21 mol of TCO_2 , making it difficult to close our budget.

491 **5.5. Potential impact of sea ice growth and ikaite export on aragonite saturation state of the**
492 **underlying seawater.**

493 The Arctic Ocean is a region where calcifying organisms are particularly vulnerable to ocean
494 acidification since low temperatures and low salinity lower the carbonate saturation state. As a result
495 several areas of the Arctic Ocean are already undersaturated with respect to aragonite (Chierici and
496 Fransson 2009; Yamamoto-Kawai et al., 2009; Bates et al., 2011). This undersaturation is enhanced in
497 winter as the temperature decreases and pCO_2 increases as a result of respiration. Calcifying organisms

498 might therefore be most susceptible to the effects of acidification in the winter, corresponding to the
499 annual minimum in aragonite saturation state ($\Omega_{\text{aragonite}}$). Sea ice retreat is thought to enhance the impact
500 of ocean acidification by freshening and ventilating the surface water (Yamamoto-Kawai et al., 2008;
501 Yamamoto et al., 2012; Popova et al., 2014). However, any understanding of the effect of ikaite
502 precipitation in sea ice on ocean acidification is still in its infancy (e.g. Fransson et al., 2013).

503 Since the discovery of ikaite precipitation in sea ice (Dieckmann et al., 2008), research on its impact on
504 the carbonate system of the underlying seawater has been ongoing. Depending on the timing and location
505 of this precipitation within sea ice, the impact for the atmosphere and the water column in terms of CO_2
506 transport can be significantly different (Delille et al., 2014). Dissolution of ikaite within melting sea ice in
507 the spring and export of this related high TA: TCO_2 ratio meltwater from the ice to the water column will
508 decrease the $p\text{CO}_2$, increase pH and $\Omega_{\text{aragonite}}$ of the surface layer seawater. Accordingly, during sea ice
509 melt, an increase of $\Omega_{\text{aragonite}}$ in the surface water in the Arctic was observed (Chierici et al., 2011,
510 Fransson et al., 2013, Bates et al., 2014). However, it was difficult to ascribe this increase to the legacy of
511 excess TA in sea ice, ikaite dissolution or primary production.

512 The impact of ikaite precipitation on the surface seawater during sea ice growth is less clear. Fransson
513 et al., (2013) suggested in winter in the Amundsen Gulf that the release of brine decreased $\Omega_{\text{aragonite}}$ by 0.8
514 at the sea ice-seawater interface as a result of ikaite precipitation within sea ice and the related CO_2
515 enrichment of brine. Conversely, during ice melt, $\Omega_{\text{aragonite}}$ increased by 1.4 between March and May,
516 likely due to both calcium carbonate dissolution and primary production. This contrasts with the present
517 experiment. Figure 10 shows the evolution of $\Omega_{\text{aragonite}}$ and pH in the water column derived from $\text{TA}_{(\text{sw})}$
518 and $\text{TCO}_{2(\text{sw})}$ and the evolution of $\Omega_{\text{aragonite}}$ and pH predicted solely from salinity changes (i.e. using
519 $\text{TA}_{(\text{sw})}^*$ and $\text{TCO}_{2(\text{sw})}^*$, noted as $\Omega_{\text{aragonite}}^*$ and pH^*). We used the CO2sys_v2.1.xls spreadsheet (Pierrot et
520 al., 2006) with the dissociation constants from Goyet and Dickson (1989) and all other constants from
521 DOE (1994). This shows the complexity of ikaite and its impact on the carbonate system and Ω in the
522 underlying water.

523 During ice growth, sea ice brine rejection appears to increase both pH (from 8.00 to 8.06) and $\Omega_{\text{aragonite}}$
524 (from 1.28 to 1.65) of the underlying seawater, offsetting the effect of decreased temperature. A slight
525 increase of $\Omega_{\text{aragonite}}$ was predicted due to increased salinity and a proportional increase of TA and TCO_2
526 as depicted in $\Omega_{\text{aragonite}}^*$. However, the effect of ikaite rejection and subsequent changes in TA strongly
527 enhance the increase of $\Omega_{\text{aragonite}}$. Therefore, ikaite rejection from sea ice has a much stronger potential to

528 increase $\Omega_{\text{aragonite}}$ than brine rejection during fall and winter sea ice growth, suggesting ikaite exported to
529 seawater from sea ice may hamper the effect of oceanic acidification on $\Omega_{\text{aragonite}}$ in fall and winter in at
530 the time when $\Omega_{\text{aragonite}}$ is at its minimum (Chierici and Fransson 2009, Yamamoto-Kawai et al., 2009,
531 Chierici et al., 2011). Ice formation may therefore delay harmful effects of ocean acidification on
532 calcifying organisms by increasing $\Omega_{\text{aragonite}}$ in the critical winter period when $\Omega_{\text{aragonite}}$ reaches its minimal
533 values. As a corollary, ice removal acts to alleviate the effect of ikaite rejection and may therefore lowers
534 $\Omega_{\text{aragonite}}$. This calls for an accounting of under-ice ikaite rejection in modeling predictions on the
535 consequences of Arctic Ocean acidification in the context of northern hemispheric annual multi-year sea
536 ice loss, as increased summer open water will lead to more first year sea ice formation in fall and winter
537 in the future.

538 6. Conclusion

539 We quantified the evolution of inorganic carbon dynamics from initial sea ice formation to its melt in
540 a sea ice-seawater mesocosm pool from 11 to 29 January 2013. Based on our analysis of TA and TCO_2 in
541 sea ice and seawater, the main processes affecting inorganic carbon within sea ice are ikaite precipitation
542 and CO_2 exchange with the atmosphere, while in the underlying seawater dissolution of ikaite was the
543 main process affecting the inorganic carbon system.

544 During this experiment, sea ice exchanged inorganic carbon components (e.g. CO_2 , ikaite, TCO_2) with
545 both the atmosphere and the underlying seawater. During sea ice growth, CO_2 was released to the
546 atmosphere while during ice melt an uptake of atmospheric CO_2 was observed. We report ikaite
547 precipitation up to $167 \mu\text{mol kg}^{-1}$ of sea ice, similar to previous estimates from Rysgaard et al., (2014)
548 based on microscopically observed values. In the underlying seawater, a net increase of $nTA_{(\text{sw})}$ over the
549 whole experiment was observed (up to $128 \mu\text{mol kg}^{-1}$), suggesting that a portion of the ikaite crystals
550 precipitated within sea ice were exported to the underlying seawater and then dissolved as the ice cover
551 evolved in time. Ikaite export from ice to the underlying seawater was associated with brine rejection
552 during sea ice growth, increased sea ice vertical connectivity due to the upward percolation of seawater,
553 and meltwater flushing during sea ice melt. Rysgaard et al., (2007) suggested that ikaite precipitation
554 within sea ice could act as a significant sink for atmospheric CO_2 , however to act as a sink for
555 atmospheric CO_2 , ikaite crystals must remain in the ice structure while the CO_2 produced by their
556 precipitation is expelled with dense brine rejection and entrained in deep seawater (Delille et al., 2014).
557 TA changes observed in the water column once the sea ice started to melt indicate that more than half of

558 the total amount of ikaite precipitated in the ice during the sea ice growth remained in the ice until the sea
559 ice began to melt. Derivation of air-sea CO₂ fluxes related to the sea ice carbon pump should take into
560 account ikaite export to the underlying ocean during sea ice growth, which might reduce the efficiency of
561 oceanic CO₂ uptake upon sea ice melt. As sea ice melts, ikaite is flushed downward out of the ice along
562 with the meltwater.

563 Ikaite export from sea ice and its dissolution had a strong impact on the underlying seawater. In this
564 semi-closed system, sea ice growth increased the seawater salinity, TA_(sw), and TCO_{2(sw)}. In spite of those
565 increases, the *p*CO₂ of the underlying seawater remained undersaturated compared to the atmosphere. We
566 conclude that ikaite dissolution within the water column is responsible for the seawaters' continual *p*CO₂
567 undersaturation. In addition, we discuss that dissolution of ikaite crystals exported from sea ice in the
568 underlying seawater can potentially hamper the effect of oceanic acidification on $\Omega_{\text{aragonite}}$ in fall and
569 winter in ice-covered areas at the time when $\Omega_{\text{aragonite}}$ is smallest.

570 **7. Acknowledgments**

571 We gratefully acknowledge the contributions of the Canada Excellence Research Chair (CERC) and
572 Canada Research Chair (CRC) programs. Support was also provided by the Natural Sciences and
573 Engineering Research Council (NSERC), the Canada Foundation for Innovation and the University of
574 Manitoba. R.J.G. thanks the NSERC Discovery Grant program. B.D. is a research associate researcher of
575 the F.R.S.-FNRS. This work is a contribution to the ArcticNet Networks of Centre of Excellence
576 and the Arctic Science Partnership (ASP) asp-net.org.

577 **8. References**

578 Bates, N. R., Cai, W. J., and Mathis, J. T.: The ocean carbon cycle in the western Arctic Ocean: Distributions
579 and air-sea fluxes of carbon dioxide, *Oceanography*, 24, 186-201, 2011.

580 Bates, N. R. and Mathis, J. T.: The Arctic Ocean marine carbon cycle: evaluation of air-sea CO₂ exchanges,
581 ocean acidification impacts and potential feedbacks, *Biogeosciences*, 6, 2433-2459, 2009.

582 Bates, N. R., Garley, R., Frey, K. E., Shake, K. L., Mathis, J. L.: Sea-ice melt CO₂-carbonate chemistry in the
583 western Arctic Ocean: meltwater contribution to air-sea CO₂ gas exchange, mixed-layer properties and rates of
584 net community production under sea ice, *Biogeosciences*, 11, 6769-6789, doi:10.5194/bg-11-6769-2014, 2014.

585 Chierici, M. and Fransson, A.: Calcium carbonate saturation in the surface water of the Arctic Ocean:
586 undersaturation in freshwater influenced shelves, *Biogeosciences*, 6, 2421-2431, 2009.

587 Chierici, M., Fransson, A., Lansard, B., Miller, L. A., Mucci, A., Shadwick, E., Thomas, E., Tremblay, J. E. and
588 Papakyriakou, T.: The impact of biogeochemical processes and environmental factors on the calcium carbonate
589 saturation state in the Circumpolar Flaw Lead in the Amundsen Gulf, Arctic Ocean, *Journal of Geophysical*
590 *Research-Oceans*, 116, C00G09, doi:10.1029/2011JC007184, 2011.

591 Copin Montégut, C.: A new formula for the effect of temperature on the partial pressure of carbon dioxide in
592 seawater, *Marine Chemistry*, 25, 29-37, 1988.

593 Cox, G. F. N. and Weeks, W. F.: Equations for determining the gas and brine volumes in sea-ice samples,
594 *Journal of Glaciology*, 29, 306 - 316, 1983.

595 Delille, B., Vancoppenolle, M., Geilfus, N.-X., Tilbrook, B., Lannuzel, D., Schoemann, V., Becquevort, S.,
596 Carnat, G., Delille, D., Lancelot, C., Chou, L., Dieckmann, G. S., and Tison, J.-L.: Southern Ocean CO₂ sink:
597 The contribution of the sea ice, *Journal of Geophysical Research: Oceans*, 119, 6340-6355, 2014.

598 Dieckmann, G. S., Nehrke, G., Papadimitriou, S., Gottlicher, J., Steininger, R., Kennedy, H., Wolf-Gladrow, D.,
599 and Thomas, D. N.: Calcium carbonate as ikaite crystals in Antarctic sea ice, *Geophysical Research Letters*, 35,
600 2008.

601 DOE (Ed.): Handbook of methods for the analysis of the various parameters of the carbon dioxide system in sea
602 water, 1994.

603 Ducklow, H. W.: Seasonal production and bacterial utilization of DOC in the Ross Sea, Antarctica, *Biogeochem.*
604 Ross Sea, vol 78, 143-158, 2003.

605 Else, B. G. T., Galley, R. J., Lansard, B., Barber, D. G., Brown, K., Miller, L. A., Mucci, A., Papakyriakou, T.
606 N., Tremblay, J. E., and Rysgaard, S.: Further observations of a decreasing atmospheric CO₂ uptake capacity in
607 the Canada Basin (Arctic Ocean) due to sea ice loss, *Geophysical Research Letters*, 40, 1132-1137, 2013.

608 Else, B. G. T., Papakyriakou, T., Galley, R., Drennan, W. M., Miller, L. A., and Thomas, H.: Wintertime CO₂
609 fluxes in an Arctic polynya using eddy covariance: Evidence for enhanced air-gas transfer during ice formation,
610 *Journal of Geophysical Research*, 116, 2011.

611 Else, B. G. T., Rysgaard, S., Attard, K., Campbell, K., Crabeck, O., Galley, R. J., Geilfus, N. X., Lemes, M.,
612 Lueck, R., Papakyriakou, T., and Wang, F.: Under-ice eddy covariance flux measurements of heat, salt,

613 momentum, and dissolved oxygen in an artificial sea ice pool, *Cold Regions Science and Technology*, 119, 158-
614 169, 2015.

615 Frankignoulle, M.: *Field-Measurements of Air Sea CO₂ Exchange*, *Limnology and Oceanography*, 33, 313-322,
616 1988.

617 Fransson, A., Chierici, M., Miller L. A., Carnat G., Shadwick, E., Thomas, H., Pineault, S. and Papakyriakou, T.
618 N.: Impact of sea-ice processes on the carbonate system and ocean acidification at the ice-water interface of the
619 Amundsen Gulf, *Arctic Ocean, Journal of Geophysical Research: Oceans*, 118, 7001-7023, 2013.

620 Galley, R. J., Else, B. G. T., Geilfus, N. X., Hare, A. A., Isleifson, D., Barber, D. G., and Rysgaard, S.: *Imaged*
621 *brine inclusions in young sea ice-Shape, distribution and formation timing*, *Cold Regions Science and*
622 *Technology*, 111, 39-48, 2015.

623 Garneau, M. E., Vincent, W. F., Alonso-Sáez L., Gratton, Y., Lovejoy, C.: *Prokaryotic community structure and*
624 *heterotrophic production in a river-influenced coastal arctic ecosystem*, *Aquat. Microb. Ecol.*, 32, 27-40, 2006.

625 Geilfus, N. X., Carnat, G., Dieckmann, G. S., Halden, N., Nehrke, G., Papakyriakou, T., Tison, J. L., and Delille,
626 B.: *First estimates of the contribution of CaCO₃ precipitation to the release of CO₂ to the atmosphere during*
627 *young sea ice growth*, *Journal of Geophysical Research*, 118, 2013a.

628 Geilfus, N. X., Carnat, G., Papakyriakou, T., Tison, J. L., Else, B., Thomas, H., Shadwick, E., and Delille, B.:
629 *Dynamics of pCO₂ and related air-ice CO₂ fluxes in the Arctic coastal zone (Amundsen Gulf, Beaufort Sea)*,
630 *Journal of Geophysical Research-Oceans*, 117, 2012.

631 Geilfus, N. X., Galley, R. J., Cooper, M., Halden, N., Hare, A., Wang, F., Søgaard, D. H., and Rysgaard, S.:
632 *Gypsum crystals observed in experimental and natural sea ice*, *Geophysical Research Letters*, doi:
633 10.1002/2013GL058479, 2013b. 2013GL058479, 2013b.

634 Geilfus, N. X., Galley, R. J., Crabeck, O., Papakyriakou, T., Landy, J., Tison, J. L., and Rysgaard, S.: *Inorganic*
635 *carbon dynamics of melt-pond-covered first-year sea ice in the Canadian Arctic*, *Biogeosciences*, 12, 2047-2061,
636 2015.

637 Geilfus, N. X., Tison, J. L., Ackley, S. F., Galley, R. J., Rysgaard, S., Miller, L. A., and Delille, B.: *Sea ice pCO₂*
638 *dynamics and air-ice CO₂ fluxes during the Sea Ice Mass Balance in the Antarctic (SIMBA) experiment -*
639 *Bellingshausen Sea, Antarctica*, *The Cryosphere*, 8, 2395-2407, 2014.

640 Golden, K. M., Eicken, H., Heaton, A. L., Miner, J., Pringle, D. J., and Zhu, J.: Thermal evolution of
641 permeability and microstructure in sea ice, *Geophysical Research Letters*, 34, 2007.

642 Goyet, C. and Poisson, A.: New determination of carbonic acid dissociation constants in seawater as a function
643 of temperature and salinity, *Deep-Sea Research Part a-Oceanographic Research Papers*, 36, 1635-1654, 1989.

644 Grasshoff, K., Ehrhardt, M., and Kremling, K.: *Methods of sea water analysis*, Verlag Chemie, 1983. 1983.

645 Hansen, J. W., Thamdrup, B., and Jørgensen, B. B.: Anoxic incubation of sediment in gas-tight plastic bags: a
646 method for biogeochemical processes studies, *Marine Ecology-Progress Series*, 208, 273-282, 2000.

647 Haraldsson, C., Anderson, L. G., Hasselov, M., Hulth, S., and Olsson, K.: Rapid, high-precision potentiometric
648 titration of alkalinity in ocean and sediment pore waters, *Deep sea Research I*, 44, 2031-2044, 1997.

649 Hare, A. A., Wang, F., Barber, D., Geilfus, N. X., Galley, R. J., and Rysgaard, S.: pH Evolution in sea ice grown
650 at an outdoor experimental facility, *Marine Chemistry*, 154, 46-54, 2013.

651 Johnson, K. M., Sieburth, J. M., Williams, P. J. L., and Brandstrom, L.: Coulometric total carbon-dioxide
652 analysis for marine studies – automation and calibration, *Marine Chemistry*, 21, 117-133, 1987.

653 Killawee, J. A., Fairchild, I. J., Tison, J. L., Janssens, L., and Lorrain, R.: Segregation of solutes and gases in
654 experimental freezing of dilute solutions: Implications for natural glacial systems, *Geochimica Et Cosmochimica
655 Acta*, 62, 3637-3655, 1998.

656 Kirchmann, D. L.: Leucine incorporation as a measure of biomass production by heterotrophic bacteria.
657 *Handbook of Methods in Aquatic Microbial Ecology*, Chap. 58, 509-518, 1993.

658 Kirchmann, D. L.: Measuring bacterial biomass production and growth rates from Leucine incorporation in
659 natural aquatic environments. *Methods in Microbiology*, Chap. 12, 227-237, 2001.

660 Leppäranta, M. and Manninen, T.: The brine and gas content of sea ice with attention to low salinities and high
661 temperatures, Helsinki, 1988.

662 Loose, B., McGillis, W. R., Perovich, D., Zappa, C. J., and Schlosser, P.: A parameter model of gas exchange for
663 the seasonal sea ice zone, *Ocean Science*, 10, 17-28, 2014.

664 MacGilchrist, G. A., Garabato, A. C. N., Tsubouchi, T., Bacon, S., Torres-Valdes, S., and Azetsu-Scott, K.: The
665 Arctic Ocean carbon sink, *Deep-Sea Research Part I-Oceanographic Research Papers*, 86, 39-55, 2014.

666 Miller, L. A., Papakyriakou, T., Collins, R. E., Deming, J., Ehn, J., Macdonald, R. W., Mucci, A., Owens, O.,
667 Raudsepp, M., and Sutherland, N.: Carbon Dynamics in Sea Ice: A Winter Flux Time Series, *Journal of*
668 *Geophysical Research-Oceans*, 116, 2011.

669 Nomura, D., Eicken, H., Gradinger, R., and Shirasawa, K.: Rapid physically driven inversion of the air-sea ice
670 CO₂ flux in the seasonal landfast ice off Barrow, Alaska after onset surface melt, *Continental Shelf Research*, 30,
671 1998-2004, 2010.

672 Nomura, D., Granskog, M. A., Assmy, P., Simizu, D., and Hashida, G.: Arctic and Antarctic sea ice acts as a
673 sink for atmospheric CO₂ during periods of snowmelt and surface flooding, *Journal of Geophysical Research:*
674 *Oceans*, doi: 10.1002/2013JC009048, 2013. 6511-6524, 2013.

675 Parsons T. R., Maita Y., Lali C. M.: *A manual of chemical and biological methods for seawater analysis*.
676 Pergamon Press, Toronto, 1984

677 Papadimitriou, S., Kennedy, H., Kattner, G., Dieckmann, G. S., and Thomas, D. N.: Experimental evidence for
678 carbonate precipitation and CO₂ degassing during sea ice formation, *Geochimica et Cosmochimica Acta*, 68,
679 1749-1761, 2004.

680 Papakyriakou, T. and Miller, L.: Springtime CO₂ exchange over seasonal sea ice in the Canadian Arctic
681 Archipelago, *Annals of Glaciology*, 52, 2011.

682 Parmentier, F.-J. W., Christensen, T. R., Sørensen, L. L., Rysgaard, S., McGuire, A. D., Miller, P. A., and
683 Walker, D. A.: The impact of lower sea-ice extent on Arctic greenhouse-gas exchange, *Nature climate change*,
684 doi: DOI:10.1038/NCLIMATE1784, 2013. 195-202, 2013.

685 Pierrot, D., Lewis, E., and Wallace, D. W. R.: MS Excel Program Developed for CO₂ System Calculations,
686 Carbon Dioxide Information Analysis Center, Oak Ridge National Laboratory, U.S. Department of Energy, Oak
687 Ridge, Tennessee, doi: 10.3334/CDIAC/otg.CO2SYS_XLS_CDIAC105a, 2006. ORNL/CDIAC-105a. , 2006.

688 Popova, E. E., Yool, A., Aksenov, Y., Coward, A. C., and Anderson, T. R.: Regional variability of acidification
689 in the Arctic: a sea of contrasts, *Biogeosciences*, 11, 293-308, 2014.

690 Rysgaard, S., Bendtsen, J., Pedersen, L. T., Ramlov, H., and Glud, R. N.: Increased CO₂ uptake due to sea ice
691 growth and decay in the Nordic Seas, *Journal of Geophysical Research*, 114, 2009.

692 Rysgaard, S., Glud, R. N., Sejr, M. K., Bendtsen, J., and Christensen, P. B.: Inorganic carbon transport during
693 sea ice growth and decay: A carbon pump in polar seas, *Journal of Geophysical Research-Oceans*, 112, 2007.

694 Rysgaard, S., Søgaard, D. H., Cooper, M., Pu, acute, ko, M., Lennert, K., Papakyriakou, T. N., Wang, F.,
695 Geilfus, N. X., Glud, R. N., Ehn, J., McGinnis, D. F., Attard, K., Sievers, J., Deming, J. W., and Barber, D.:
696 Ikaite crystal distribution in winter sea ice and implications for CO₂ system dynamics, *The Cryosphere*, 7, 707-
697 718, 2013.

698 Rysgaard, S., Wang, F., Galley, R. J., Grimm, R., Notz, D., Lemes, M., Geilfus, N. X., Chaulk, A., Hare, A. A.,
699 Crabeck, O., Else, B. G. T., Campbell, K., Sørensen, L. L., Sievers, J., and Papakyriakou, T.: Temporal
700 dynamics of ikaite in experimental sea ice, *The Cryosphere*, 8, 1469-1478, 2014.

701 Sabine, C. L., Feely, R. A., Gruber, N., Key, R. M., Lee, K., Bullister, J. L., Wanninkhof, R., Wong, C. S.,
702 Wallace, D. W. R., Tilbrook, B., Millero, F. J., Peng, T. H., Kozyr, A., Ono, T., and Rios, A. F.: The oceanic
703 sink for anthropogenic CO₂, *Science*, 305, 367-371, 2004.

704 Sejr, M. K., Krause-Jensen, D., Rysgaard, S., Sørensen, L. L., Christensen, P. B., and Glud, R. N.: Air-sea flux
705 of CO₂ in arctic coastal waters influenced by glacial melt water and sea ice, *Tellus Series B Chemical and*
706 *Physical Meteorology*, 63, 815-822, 2011.

707 Semiletov, I. P., Makshtas, A., Akasofu, S. I., and Andreas, E. L.: Atmospheric CO₂ balance: The role of Arctic
708 sea ice, *Geophysical Research Letters*, 31, 2004.

709 Søgaard, D. H., Thomas, D. N., Rysgaard, S., Norman, L., Kaartokallio, H., Juul-Pedersen T., Glud, R. N. and
710 Geilfus, N. X.: The relative contributions of biological and abiotic processes to the carbon dynamics in subarctic
711 sea ice, *Polar Biol.*, doi:10.1007/s00300-013-1396-3, 2013.

712 Yamamoto, A., Kawamiya, M., Ishida, A., Yamanaka, Y., and Watanabe, S.: Impact of rapid sea-ice reduction in
713 the Arctic Ocean on the rate of ocean acidification, *Biogeosciences*, 9, 2365-2375, 2012.

714 Yamamoto-Kawai, M., McLaughlin, F. A., Carmack, E. C., Nishino, S., and Shimada, K.: Aragonite
715 Undersaturation in the Arctic Ocean: Effects of Ocean Acidification and Sea Ice Melt, *Science*, 326, 1098-1100,
716 2009.

717 Yamamoto-Kawai, M., McLaughlin, F. A., Carmack, E. C., Nishino, S., and Shimada, K.: Freshwater budget of
718 the Canada Basin, Arctic Ocean, from salinity, delta O-18, and nutrients, *Journal of Geophysical Research-*
719 *Oceans*, 113, 12, 2008.

720 Zeebe, R. E. and Wolf-Gladrow, D.: CO₂ in seawater: Equilibrium, Kinetics, Isotopes, Elsevier, 2001. 2001.

721

722 9. Table

723 Table 1: Seawater conditions on 11 January, before any sea ice formation ($t=0$), on 25 January, just
 724 before the heat was turned back on and on 29 January, at the end of the experiment. Note
 725 that seawater salinity and $TA_{(sw)}$ do not reach the initial seawater values as sea ice was still
 726 present at the end of the experiment.

Date	Temperature (°C)	Salinity	TA ($\mu\text{mol kg}^{-1}$)	$n\text{TA}$ ($\mu\text{mol kg}^{-1}$)	TCO_2 ($\mu\text{mol kg}^{-1}$)	$nTCO_2$ ($\mu\text{mol kg}^{-1}$)
11 Jan.	-1.4	33.5	2453	2416	2341	2306
25 Jan.	-1.9	35.5	2659	2471	2524	2346
29 Jan.	-0.6	34.4	2607	2500	2461	2361

727

728

729 Table 2: Masses of TCO_2 in the water column ($TCO_{2(sw)}$) and in the ice cover ($TCO_{2(ice)}$), masses of
 730 ikaite within the ice cover estimated from this study and from Rysgaard et al., (2014), masses
 731 of ikaite dissolved in the water column ($Ikaite_{(sw)}$) and masses of CO_2 exchanged between the
 732 ice and the atmosphere over the whole pool (estimation based on the air-ice CO_2 fluxes). All
 733 units are in mole.

January (DOY)	$TCO_{2(sw)}$	$TCO_{2(ice)}$	$Ikaite_{(ice)}$ <i>from this study</i>	$Ikaite_{(ice)}$ <i>from Rysgaard et al., (2014)</i>	$Ikaite_{(sw)}$	$CO_{2(air-ice)}$
t=0	1041					
13.75	1040	2.38	0.17	0.00	0.47	
13.88	1044	2.09	0.00	0.00	0.87	
14	1043	2.90	0.25	0.00	0.83	0.03
14.13	1043	3.29	0.62	0.00	2.57	0.02
14.25	1038	4.91	-0.05	0.00	1.06	0.01
14.5	1037	4.77	0.18	0.00	3.75	0.12
14.75	1039	4.36	0.12	0.05	2.73	0.07
15	1037				1.80	0.08
15.25	1032	4.67	0.98	0.68	1.28	0.01
15.5	1034	3.89	1.58	0.00	-1.57	0.07
15.92	1034	4.47	0.69	0.00	1.63	0.12
16.38	1024	7.36	1.45	0.08	3.60	0.19
16.67	1028	8.17	1.87	0.00	6.00	0.10
17.38	1023	15.48	0.29	0.65	3.90	0.22
17.67	1026	13.26	0.04	0.46	4.50	0.13
18.38	1030	11.39	0.74	2.14	5.61	0.38
18.67	1027	12.06	0.21	0.21	7.16	0.10
19.38	1029	11.13	0.01	0.84	6.96	0.23
19.67	1030	10.75	0.03	0.09	1.97	0.11
20.38	1028	10.25	-0.12	0.23	1.47	0.42
20.67	1022	10.36	-0.70	0.71	3.48	0.12
21.38	1025	10.50	0.88	0.35	7.42	0.35
23.63	1034	12.60	1.34	2.14	11.18	
24.38	1026	14.84	1.30	1.94	9.75	0.21
25.38	1017	15.67	1.09	3.05	6.62	
25.5	1029				11.51	0.02
28.67	1022	13.46	-0.57	0.46	20.91	-0.93
29.38	987.3	15.82	-0.56	0.55	26.72	-0.15

10. Figure Captions

Figure 1: The Sea Ice Environmental Research Facility with thin sea ice covering the pond during the 2013 experiment. Photo: J. Sievers.

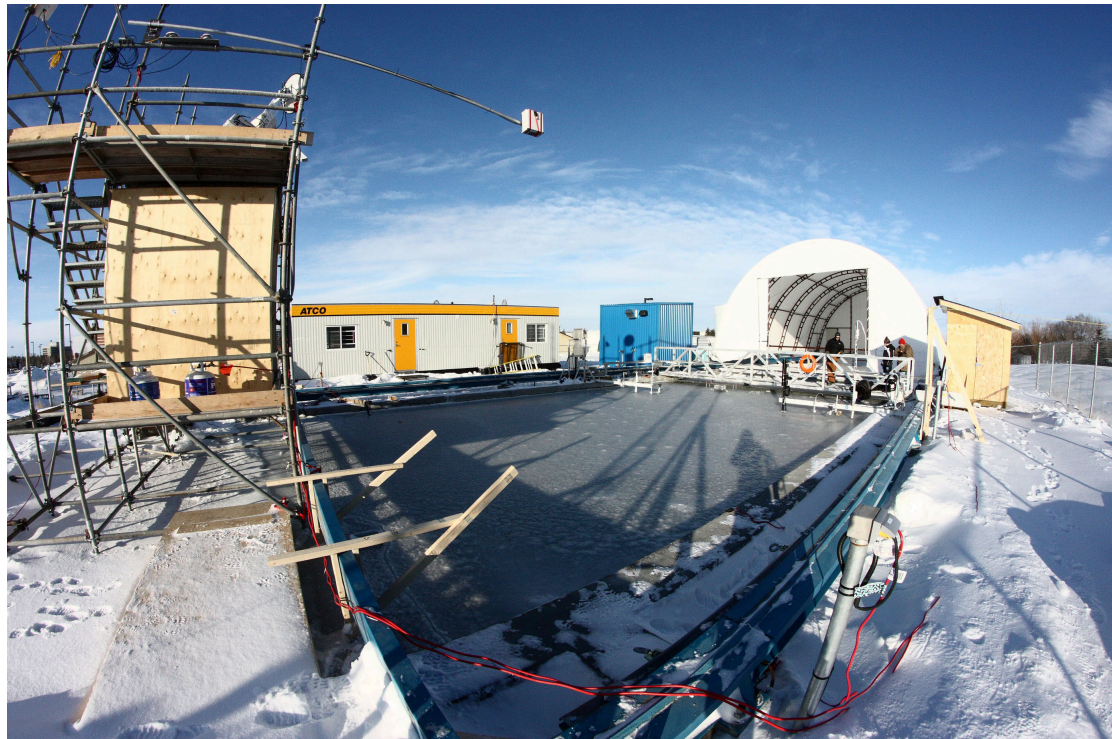


Figure 2: Evolution of (a) Air temperature ($^{\circ}\text{C}$) at 2 m height, (b) snow thickness (black shaded areas) and sea ice/seawater temperature ($^{\circ}\text{C}$), (c) bulk ice salinity, (d) brine volume content within sea ice, (e) seawater temperature (blue) and salinity (green). Measurements were performed at 30, 100, 175 and 245 cm water depths. The darker the color is, the closer to the surface. In panels (b), (c), (d) sea ice thickness is illustrated by black dots. Stars on panel (b) represent the depth at which the temperature profiles are derived from. Open squares in the lower part of (d) mark the sampling times. The dashed line on panel (e) indicates when the heat at the bottom of the pool was turned back on.

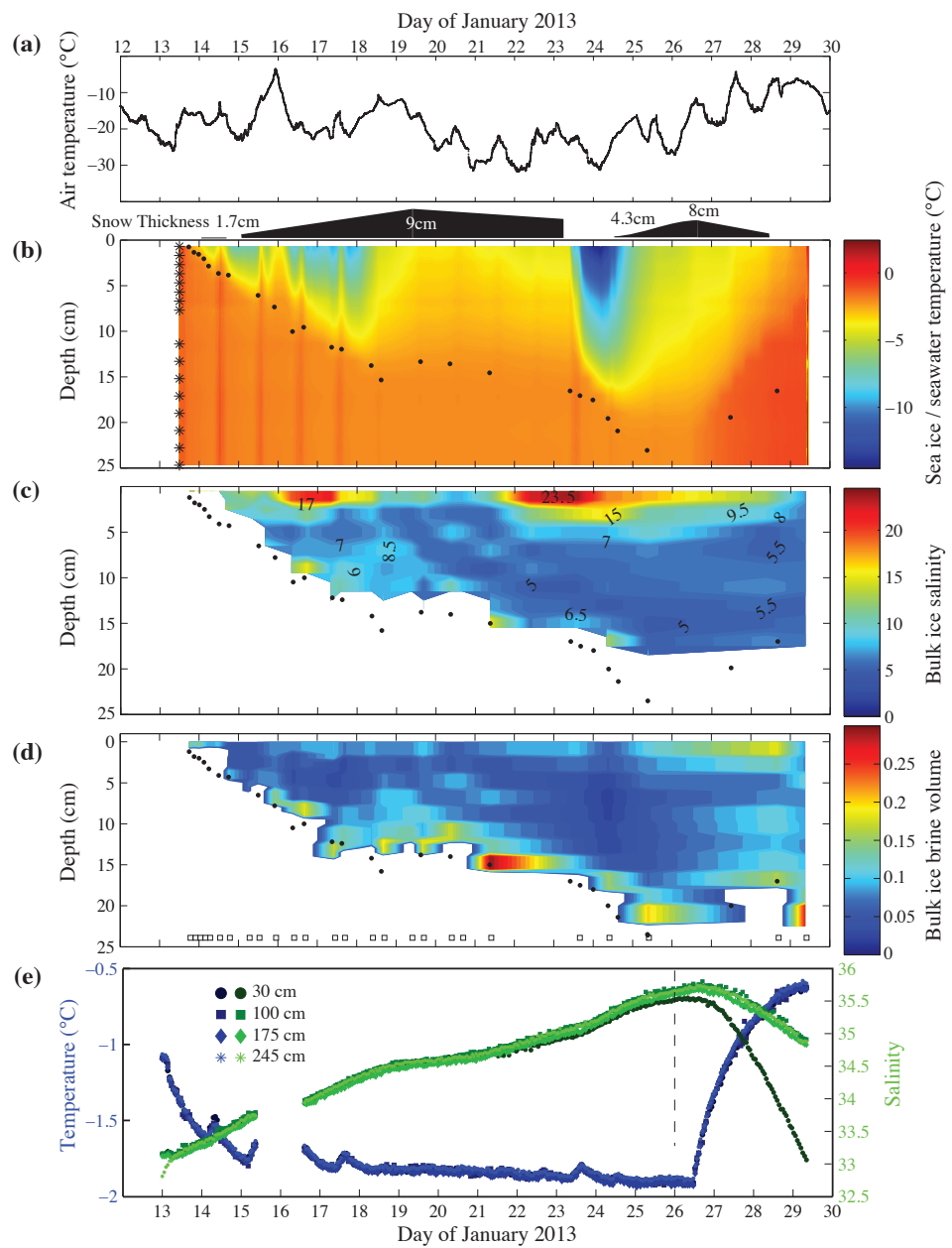


Figure 3: Evolution of (a) $TA_{(sw)}$ and $TA_{(sw)}^*$ ($\mu\text{mol kg}^{-1}$), (b) $TCO_{2(sw)}$ and $TCO_{2(sw)}^*$ ($\mu\text{mol kg}^{-1}$), (c) $nTA_{(sw)}$ (black) and $nTCO_{2(sw)}$ (green) ($\mu\text{mol kg}^{-1}$) and (d) the seawater $p\text{CO}_2$ (μatm) measured in situ (black) and corrected to a constant temperature of -1°C (blue). In panels (a) and (b) the black line is the average over the three depths while the dotted red line is the expected concentrations according to the variation of salinity observed and calculated from the mean values of the three depths ($TA_{(sw)}^*$ and $TCO_{2(sw)}^*$, respectively). The vertical black dotted line on 26 January mark when the heat was turned back ON.

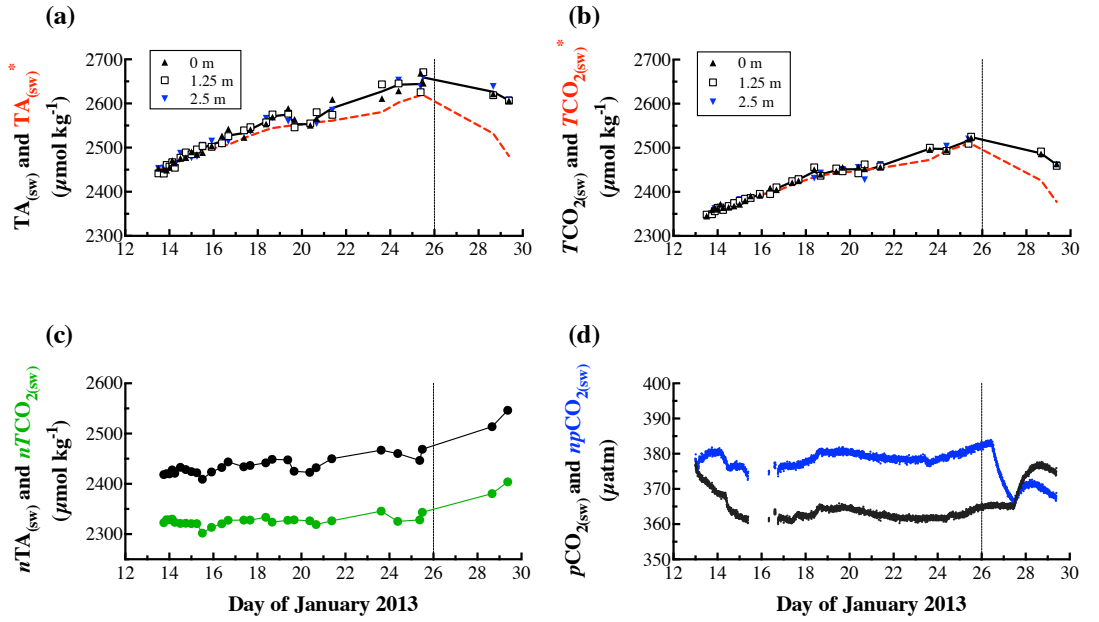


Figure 4: Evolution of (a) $TA_{(ice)}$ ($\mu\text{mol kg}^{-1}$), (b) $TCO_2_{(ice)}$ ($\mu\text{mol kg}^{-1}$), (c) $nTA_{(ice)}$ ($\mu\text{mol kg}^{-1}$) and (d) $nTCO_2_{(sw)}$ ($\mu\text{mol kg}^{-1}$). Sea ice thickness is illustrated by black dots. Open squares in the lower part of (d) mark the sampling times.

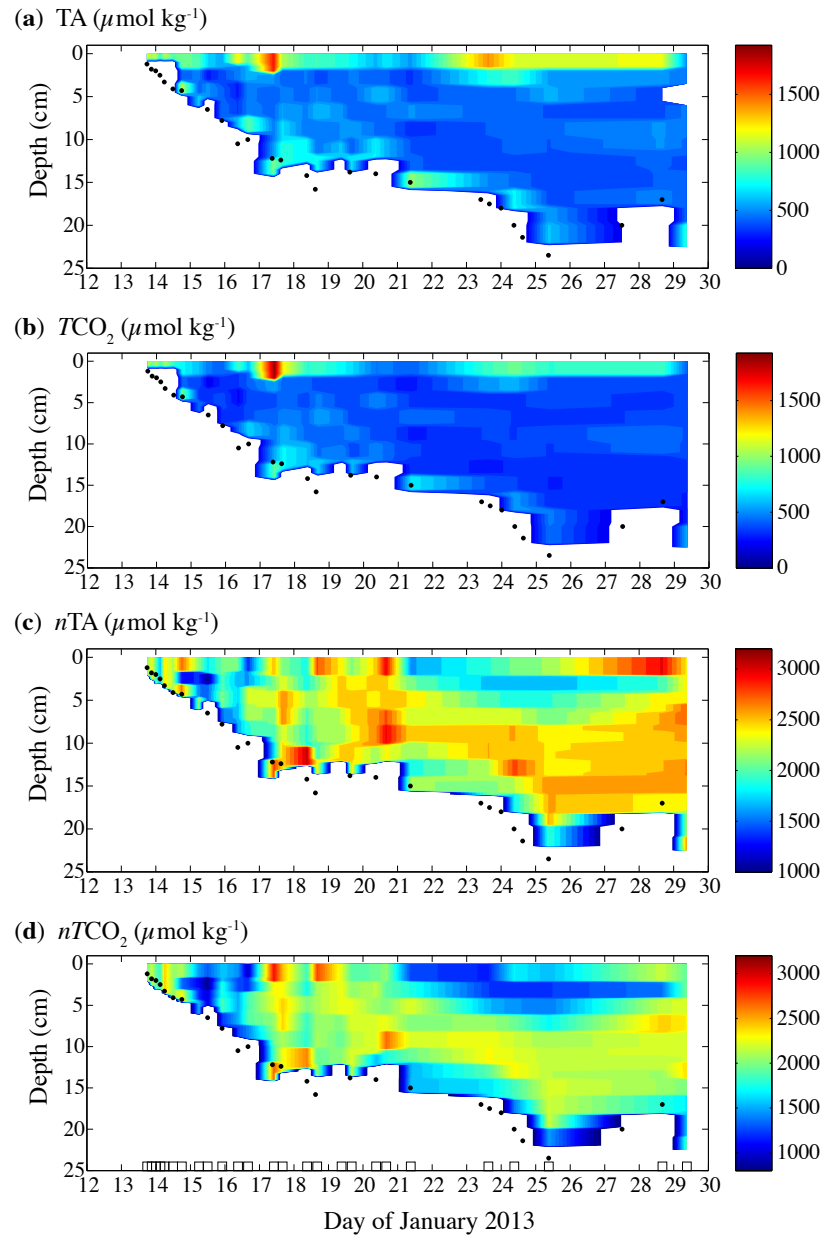


Figure 5: Air-ice CO_2 fluxes ($\text{mmol m}^{-2} \text{d}^{-1}$). Positive air-ice CO_2 flux means outgassing from the ice and negative CO_2 flux means uptake of atmospheric CO_2 . The vertical black dotted line on 26 January mark when the heat was turned back ON.

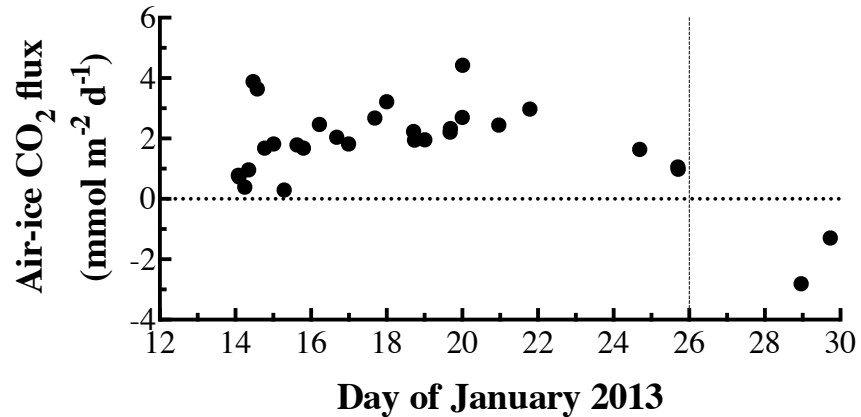


Figure 6: (a) Relationship between $n\text{TCO}_2$ and $n\text{TA}$ ($\mu\text{mol kg}^{-1}$) in bulk sea ice (white hexagons) and seawater (black dots), (b) Zoom on seawater data. The different dotted lines represent the theoretical evolution of $n\text{TA}$ and $n\text{TCO}_2$ ratio following the precipitation/dissolution of calcium carbonate and release/uptake of $\text{CO}_{2(g)}$. A linear regression is shown in green for the ice samples (a) and blue for seawater samples (b).

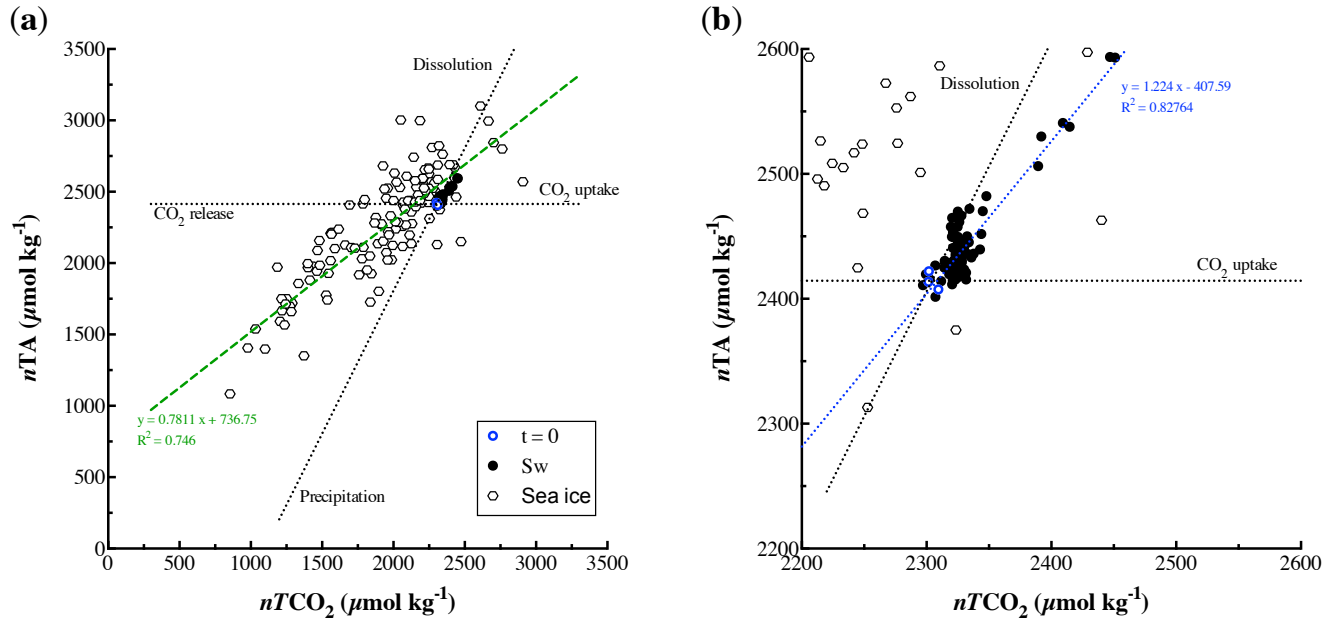


Figure 7: Evolution of (a) $TA_{(ice)}$ averaged throughout the ice thickness at each sampling day (black dots) and $TA_{(ice)}^*$ (dashed red line) ($\mu\text{mol kg}^{-1}$) and (b) $TCO_{2(ice)}$ averaged throughout the ice thickness at each sampling day (black diamonds) and $TCO_{2(ice)}^*$ (dashed red line) ($\mu\text{mol kg}^{-1}$), (c) Estimation of the ikaite precipitation/dissolution from half of the difference between $TA_{(ice)}^*$ and $TA_{(ice)}$ ($\mu\text{mol kg}^{-1}$) (black diamonds) compared to the average amount of ikaite precipitated throughout the ice thickness for each sampling day from Rysgaard et al., (2014) (white dots). The vertical black dotted line on 26 January mark when the heat was turned back ON.

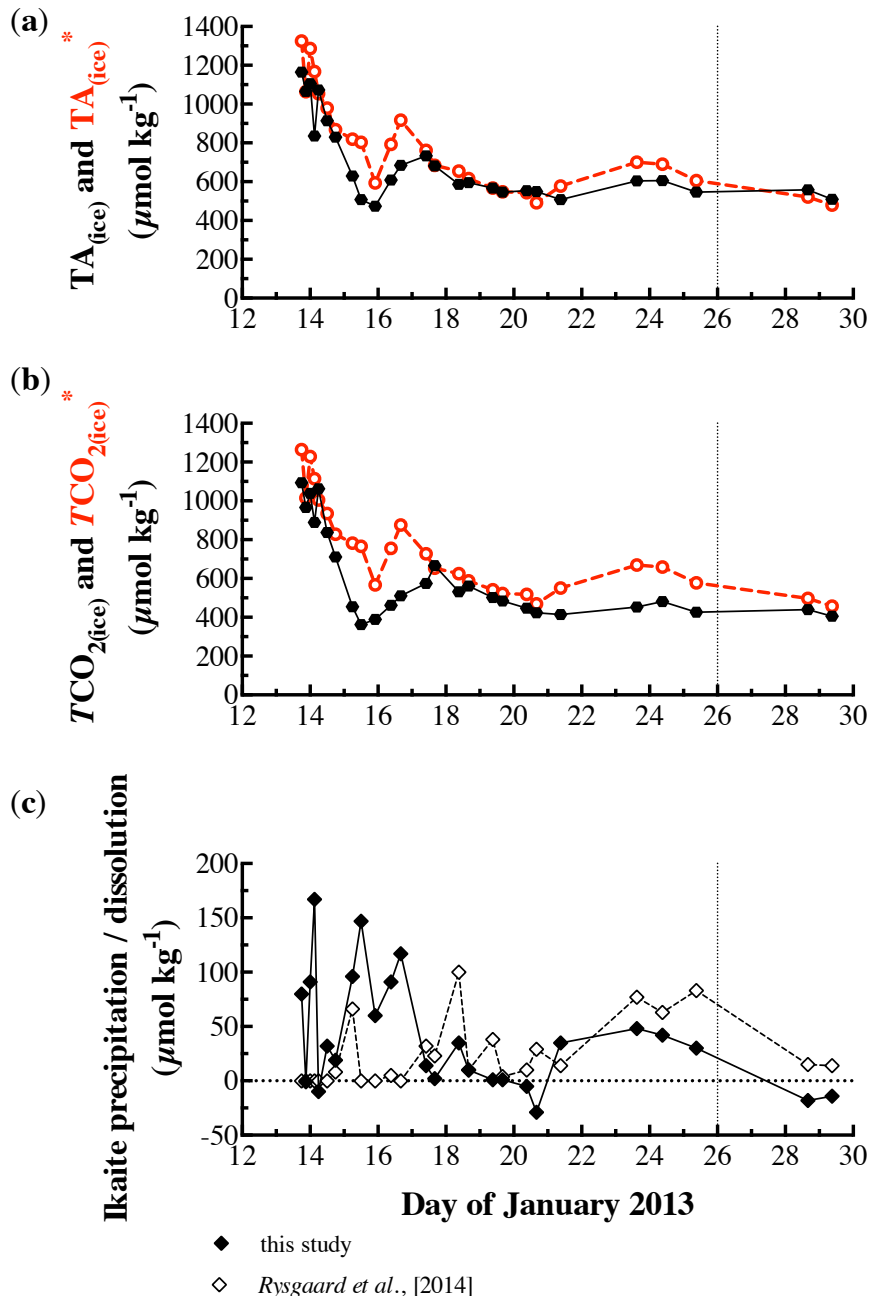


Figure 8: Evolution of (a) ikaite dissolution within the water column (in $\mu\text{mol kg}^{-1}$), (b) mass of ikaite dissolved in the underlying seawater (blue), mass of ikaite precipitated in sea ice (black) estimated from this study and estimated from Rysgaard et al., (2014) (white). The vertical black dotted line on 26 January mark when the heat was turned back on.

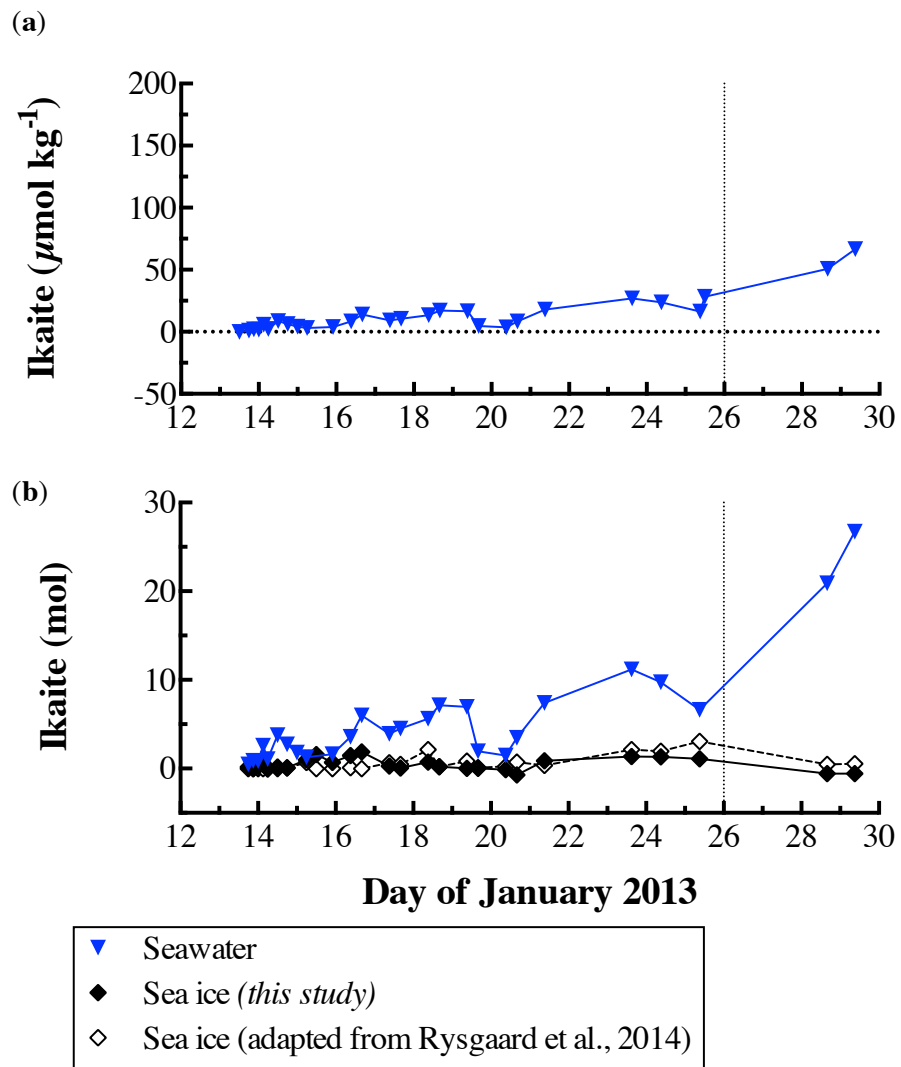


Figure 9: Total amount of TCO_2 lost from the ice cover (black dots), amount of CO_2 exchanges between the atmosphere and the ice cover ($CO_{2air-ice}$, white triangle) and sea ice-seawater TCO_2 exchanges (blue triangle). In mole for each day, integrated over the whole tank. The dotted line on 26 January mark when the heat was turned back ON.

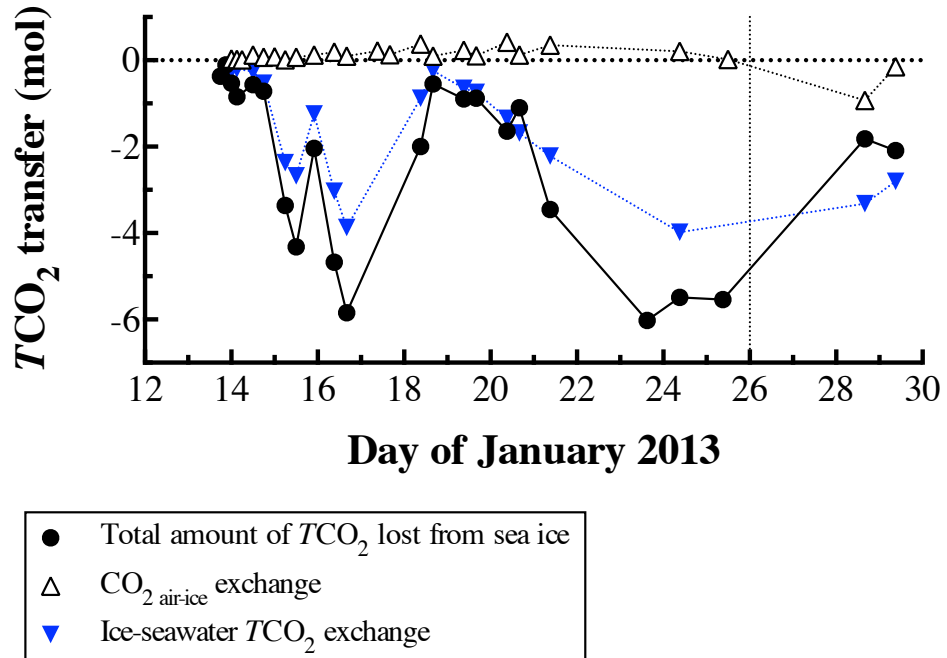


Figure 10: Evolution of (a) $\Omega_{\text{aragonite}}$ in the water column, calculated based on $\text{TA}_{\text{(sw)}}$ and $\text{TCO}_{2\text{(sw)}}$ (black dots) and calculated based on $\text{TA}_{\text{(sw)}}^*$ and $\text{TCO}_{2\text{(sw)}}^*$ (dashed red line) and (b) pH in the water column calculated based on $\text{TA}_{\text{(sw)}}$ and $\text{TCO}_{2\text{(sw)}}$ (black dots) and calculated based on $\text{TA}_{\text{(sw)}}^*$ and $\text{TCO}_{2\text{(sw)}}^*$ (dashed red line).

